Circulation of Winter Water on the Chukchi Shelf in Early Summer

Robert S. Pickart[1], G.W.K. Moore[2], Chongyuan Mao[3*], Frank Bahr[1], C. Nobre[1], Thomas J. Weingartner[4],

Submitted to Deep-Sea Research II, May 2015

Corresponding Author: R. Pickart (rpickart@whoi.edu)

[1]Woods Hole Oceanographic Institution; Woods Hole, MA, USA.

[2]University of Toronto; Toronto, Ontario, CA.

[3]National Oceanography Centre; Southampton, UK.

[*]Now at: Met Office, FitzRoy Road, Exeter, Devon, UK

[4]School of Fisheries and Ocean Sciences, University of Alaska; Fairbanks, USA.

Abstract

Using a variety of data sources we investigate the properties and pathways of Pacific-origin winter water as it spreads across the eastern Chukchi shelf in early summer. The focus is on the time period June-July 2011 during which an extensive shipboard hydrographic/velocity survey was undertaken as part of the Impacts of Climate on Ecosystem and Chemistry of the Arctic Pacific Environment (ICESCAPE) program. A revised circulation scheme is constructed revealing that the transport pathways on the Chukchi shelf are more complex than previously thought. Notably, the well known branch progressing northward from the Central Channel bifurcates as it reaches Hanna Shoal, flowing around both sides of the shoal and dividing into smaller filaments that continue towards Barrow Canyon. Mass is conserved in the circulation scheme, with approximately 1 Sverdrup flowing poleward across the Chukchi shelf within these pathways, then exiting Barrow Canyon. The salinity of the winter water varied on the shelf in 2011, with saltier water found in the upstream portion of what is defined as the central pathway. Using sea ice concentration data and atmospheric reanalysis fields, we argue that salinization of the winter water in the central pathway occurred via brine rejection as the parcels progressed north and passed through the Cape Lisburne polynya. This demonstrates that winter water pervading the interior shelf can be transformed by convective overturning north of Bering Strait, presumably stirring up nutrients from the sediments and thereby influencing primary productivity in the region of Hanna Shoal.

1. Introduction

Pacific water enters the Arctic Ocean through Bering Strait and flows northward across the wide and shallow Chukchi Sea. The characteristics of the water vary strongly with season, from warm and fresh water in summer to relatively salty and very cold water in winter and early-spring. The winter water is formed because of ice growth, which densifies the surface layer and leads to convective overturning that reaches the bottom. As such, the water is near the freezing point, weakly stratified, and high in nutrients that were stirred into the water column from the sediments. These properties together exert a strong influence on the physical state and ecosystem of the western Arctic Ocean. The dense winter water ventilates the upper halocline of

the Canada Basin (Aagaard et al., 1981), its vorticity structure influences the manner in which the water is fluxed off the Chukchi and Beaufort shelves (Pickart et al., 2005; Spall et al., 2008), and the high nitrate concentration fuels primary productivity throughout the region (e.g. Hill et al., 2005). Hence, it is of high importance to determine the precise pathways, mixing, and residence time of the winter water as it traverses the Chukchi shelf, none of which are presently well known.

Based on mooring data obtained through the years, and various numerical modeling studies, the basic circulation pattern of the Chukchi Sea has become more clearly defined. To first order the flow is dictated by the bottom topography of the Chukchi shelf (Figure 1). North of Bering Strait the Pacific water is steered into three main branches: the western branch flows through Hope Valley into Herald Canyon, the middle branch flows through the topographic depression between Herald Shoal and Hanna Shoal known as Central Channel, and the eastern branch follows the coastline of Alaska towards Barrow Canyon. In summer and early-fall the eastern branch is referred to as the Alaskan Coastal Current (Paquette and Bork, 1974), advecting the warm and fresh coastal water originating from the eastern Bering Sea and Gulf of Alaska. Recent evidence suggests that, at this time of year, most of the inflowing transport through Bering Strait is carried by this current together with the Central Channel branch (Gong and Pickart, 2015; Itoh et al., 2015). Averaged over the entire year, however, it is argued that the western branch transports roughly 50% of the Pacific water (some of which gets diverted through Long Strait into the East Siberian Sea), while the other two branches transport roughly 25% each (Woodgate et al., 2005). Modeling studies indicate a similar annually averaged partitioning of the flow (Winsor and Chapman, 2004; Spall, 2007).

Winds influence the circulation on the Chukchi shelf significantly on a variety of timescales. Woodgate et al. (2005) demonstrated that the dominant observed variability in velocity over most of the shelf is due to changes in the large-scale wind field (with the exception of Herald Canyon). Assimilating Woodgate et al.'s (2005) mooring data and other available in-situ data into a diagnostic model, Panteleev et al. (2010) showed how the shelf circulation is sensitive to the seasonal wind patterns. During mid- to late-autumn, when the winds tend to be strongly out of the northeast, more of the inflowing Pacific water is diverted towards Herald Canyon. This is

consistent with the numerical model results of Winsor and Chapman (2004) and also with the inferences of Weingartner et al., (1998) based on data from the eastern shelf. In contrast, during spring when the winds weaken, the flow is more evenly distributed among the three branches. On shorter timescales the currents in the two canyons that cut into the shelf – Barrow Canyon in the east and Herald Canyon in the west – are strongly influenced by synoptic weather systems. Upwelling and reversed flow to the south readily occur in both canyons (Aagaard and Roach 1990; Pickart et al., 2010).

The detailed circulation and ultimate fate of the Pacific water in the northern part of the Chukchi shelf remain somewhat vague at this point. Numerical models imply that when the wind forcing is weak much of the water ultimately ends up in Barrow Canyon (Winsor and Chapman, 2004; Spall 2007). This is because the flow generally follows bottom depth contours (Figure 1). The water in the eastern branch roughly parallels the coast of Alaska and flows directly into the canyon. After the water in the middle branch passes through Central Channel the topography steers it anti-cyclonically around Hanna Shoal towards the head of Barrow Canyon. For the western pathway, north of Herald Shoal the bathymetric contours bend to the east (Figure 1) which also brings some of the water in this branch around Hanna Shoal into Barrow Canyon. The remainder of the western branch continues northward through Herald Canyon and reaches the canyon mouth where it encounters the edge of the Chukchi shelf. This outflow is believed to form an eastward-flowing shelfbreak current (Pickart et al., 2005; Mathis et al., 2007; Pickart et al., 2010) that eventually reaches the mouth of Barrow Canyon.

The timing of the northward progression of Pacific water through the Chukchi Sea is also uncertain. Both observations and models indicate that it takes roughly 3-4 months for water to traverse from Bering Strait to the central portion of the shelf (Woodgate et al., 2005; Winsor and Chapman, 2004; Spall, 2007). Not surprisingly, it takes significantly longer for the water in the middle and western branches to reach Barrow Canyon than it does for the water in the eastern branch. Spall's (2007) model indicates an advective time of 6-8 months for the flow through Central Channel and Herald Canyon that bends to the east on the northern part of the Chukchi shelf and drains through Barrow Canyon. The simulation of Winsor and Chapman (2004) suggests that the portion of the western branch that forms the Chukchi shelfbreak jet takes more

than two years to reach the mouth of Barrow canyon. In contrast, Weingartner et al. (1998) estimate that in the summer months the swift Alaskan Coastal Current transports water from Bering Strait to the head of Barrow Canyon in just 2-3 months. It should be remembered, however, that the travel times of all of the branches are significantly longer when under the influence of northerly winds (Winsor and Chapman, 2004).

In addition to the model studies quoted above, there is observational evidence suggestive of the "long route" of Pacific water on the northern part of the Chukchi shelf. Shipboard velocity data indicate that some of the western branch through Herald Canyon is diverted to the east beyond Herald Shoal (Weingartner et al., 2005; Pickart et al., 2010). As seen in Figure 1, this flow should join the outflow from Central Channel and circulate anti-cyclonically around Hanna Shoal into Barrow Canyon. Such a clockwise flow around the shoal is suggested by limited observations (Weingartner et al., 2013a). As such, there should be eastward flow to the southeast of Hanna Shoal, and the mooring data of Weingartner et al. (2005) confirm this. Furthermore, moored temperature records at the head of Barrow Canyon have indicated the presence of Pacific winter water well into the summer season (Woodgate et al., 2005; Weingartner et al., 2005), consistent with such a long advective route. However, while supportive, the observational data to date are sparse. Consequently, the circulation pattern depicted by the models – in particular the topographically steered flow around Hanna Shoal into Barrow Canyon – remains to be confirmed using in-situ measurements.

In this paper we use data from two shipboard hydrographic/velocity/tracer surveys, in conjunction with mooring measurements, to elucidate the circulation of cold Pacific winter water on the northeast Chukchi shelf. The data were collected in late-spring / early-summer 2010 and 2011. While the observations are not synoptic, the winds were relatively steady throughout the measurement periods and so the results are not aliased by variable atmospheric forcing. Our data indicate that the winter water circulation is more complex than previously envisioned, and not entirely in line with the previous model results. We begin with a presentation of the various datasets, followed by an overview of the atmospheric conditions during the fieldwork. Then we present the characteristics and distribution of winter water on the shelf. A clear circulation pattern emerges, which elucidates the long route for winter water to reach Barrow Canyon. We define a

main pathway on the central shelf and discuss the nature and cause of the variation in water mass properties along this route.

2. Data and Methods

2.1 Shipboard Hydrographic Data

Two cruises on the USCGC *Healy* were carried out in early-summer 2010 and 2011 in the Chukchi Sea as part of the "Impacts of Climate on Ecosystem and Chemistry of the Arctic Pacific Environment" (ICESCAPE) program (Arrigo et al., 2012). The first cruise took place from 13 June − 22 July, 2010 (ICESCAPE I), and the second took place from 25 June – 29 July, 2011 (ICESCAPE II). Some of the sections were occupied on both cruises, but the lateral coverage on the second cruise was more extensive. For this reason, and to maximize synopticity, we focus on the 2011 dataset. As seen in Figure 2, the 2011 survey nicely covered the northeast Chukchi shelf, including the southern half of Barrow Canyon. For completeness we include one transect from the 2010 cruise which crosses the Central Channel, since this section was not occupied in 2011. We emphasize that both surveys took place during the same time of year (June/July), and the distribution of winter water on the shelf was very similar in each. Hence this justifies our including the 2010 Central Channel section in the study.

On both cruises a Sea-Bird 911+ conductivity/temperature/depth (CTD) instrument was mounted on a 12-position rosette with 30-liter Niskin bottles. The temperature sensors underwent laboratory calibrations before and after each cruise, and the conductivity sensors were calibrated using the in-situ salinity data. The resulting accuracies are 0.008^{o}C for temperature and 0.004 for salinity for waters on the shelf, and 0.002^{o}C and 0.002, respectively, for waters on the continental slope. During one of the transects on the 2011 cruise, expendable CTD probes were used (XCTDs). The accuracy of the XCTD data are taken to be 0.02^{o}C for temperature, 0.04 for salinity, and 1m for depth (see Kadko *et al.*, 2008). Vertical sections of potential temperature, salinity, and potential density were constructed using a Laplacian-Spline interpolator with a lateral grid spacing of 5-15 km and a vertical grid spacing of 2-5 m.

155
156 **2.2 Shipboard Velocity Data**
157
158 Velocity data were obtained on both ICESCAPE cruises using the hull-mounted Ocean
159 Surveyor 150 KHz Acoustic Doppler Current Profiler (ADCP) on *Healy*. The data were acquired
160 using the University of Hawaii's UHDAS software and were post-processed with the CODAS3
161 software package (see http://currents.soest.hawaii.edu). The two main challenges for obtaining
162 useful data were the presence of ice under the hull, which often times blocks the transducer, and
163 the occurrence of bubbles under certain conditions. The CODAS3 visual editing tools were
164 applied to minimize both of these error sources.
165
166 Low frequency (i.e. days to weeks) ADCP errors can result from the misalignment of the
167 ADCP transducer or from small errors in the ship's heading record. *Healy's* ADCP installation
168 was assessed using bottom track and water track calibrations. These compare the ship track or
169 ship's accelerations derived from the ADCP with those derived from the GPS data. The extensive
170 periods of shallow water encountered during the ICESCAPE cruises allowed for long timeseries
171 of bottom tracking. As such, the time-invariant hardware alignment was well determined, and the
172 time-dependent features of the timeseries helped quantify heading device fluctuations. The
173 resulting small bottom track standard deviation of 0.1 degrees suggests that fluctuations of the
174 ship's heading unit were small. We therefore estimate that the low-frequency ADCP errors were
175 less than 2 cm/s. Following the CODAS3 processing, the velocities were de-tided using the
176 Oregon State University barotropic tidal prediction model http://volkov.oce.orst.edu/tides
177 (Padman and Erofeeva, 2004).
178
179 The ADCP data do not extend over the full water column. There is a surface blanking region
180 of roughly 15-20 m, and a bottom blanking region of 15% of the local water depth (e.g. 7.5 m
181 for a shelf depth of 50 m). Since we are interested in the circulation of Pacific winter water
182 throughout the water column, we computed absolute geostrophic velocities by referencing the
183 thermal wind shear using the ADCP data. This was done as follows. Using the gridded vertical
184 sections of temperature and salinity, we constructed vertical sections of dynamic height (relative
185 to the sea surface). Analogous sections of velocity perpendicular to each transect were made

using the de-tided ADCP data. Then, at each cross-stream grid point across the section, the absolute geostrophic velocity was calculated by matching the vertically-integrated relative geostrophic velocity to the integrated ADCP velocity over their common depth range. This was done for the XCTD transect as well. Finally, vertical sections of absolute geostrophic velocity were constructed using the same Laplacian-Spline interpolator employed for the CTD variables.

2.3 Shipboard Nitrate data

Nutrients were measured during both cruises at standard depths (typically 6 levels for a 50 m cast). A Seal Analytical continuous-flow AutoAnalyzer 3 was used, with modifications according to Armstrong et al. (1967). Here we use only the nitrate data (NO_3^-), which were typically finalized with 24 hours of the water sample collection at a station. For detailed presentations of the ICESCAPE nutrient data see Mills et al. (2015) and Lowry et al. (2015).

2.4 Shipboard Wind Data

During the ICESCAPE cruises *Healy* had four meteorological sensors mounted on various parts of the ship, providing one-minute averaged true wind speed and direction by accounting for the motion of the vessel using the GPS data. In general, the four sensors gave similar results for both speed and direction, but the instrument located on the starboard main mast was considered to be most reliable and subject to the least amount of blocking due to the vessel's superstructure (S. Roberts, pers. comm., 2012). Accordingly, we used the data from the main mast starboard sensor. To assess the accuracy of this product, we compared it to timeseries from the meteorological station in Pt. Barrow, AK (marked by the star in Figure 3). Although the ship was often a fair distance from the weather station, the two timeseries were generally similar. During the occupation of the transect across the central part of Barrow Canyon (section BCC in Figure 2), which was the closest section to the meteorological station, the agreement was near perfect. This provides confidence in the accuracy of the wind data obtained from *Healy*.

2.5 Reanalysis Fields and Ice Concentration Data

To assess the large-scale atmospheric setting during the ICESCAPE program, and to estimate salt production due to polynya formation, we use fields from the North American Regional Reanalysis (NARR) (Mesinger et al., 2006) and sea ice concentration data from the Advanced Microwave Scanning Radiometer (AMSR-E) (Spreen et al., 2008). The spatial and temporal resolution of the NARR is 32 km and 6 hours, respectively. Previous work has shown that although the surface meteorological fields from the NARR are in good agreement with observations at high latitudes, the sensible and latent heat fluxes are biased high (Renfrew et al., 2009). As a result, we use a well-established bulk parameterization to estimate the turbulent fluxes (Smith, 1988; DeCosmo et al., 1996) with the NARR surface meteorological fields as inputs (Moore et al., 2014).

The fidelity of the radiative fluxes in all reanalyses is a function of the ability of the particular reanalysis to capture the cloud fraction (Walsh et al., 2009). In this regard, the NARR is one of the few reanalyses to correctly capture the transition in the change in sign of the net radiative forcing that occurs in the Arctic during the spring period (Walsh et al., 2009). On the other hand, in a comparison to observations at the ARM site at Point Barrow, the NARR downwelling longwave flux is biased high by ~10% during the winter and biased low by ~10% during the summer with the transition occurring in May (Walsh et al., 2009). As a result, the net longwave cooling in the NARR is underestimated during the winter and overestimated in the summer.

The spatial resolution of the daily AMSR-E ice concentration data is 6.25 km, and the values are deemed accurate to ±10% (Cavaleiri et al., 1991). For the salt production calculations, daily mean values of the NARR fields were generated and then interpolated to the AMSR-E spatial grid.

2.6 Mooring Data

2.61 Chukchi Shelf

To enhance the coverage of data on the Chukchi shelf we used timeseries from a collection of moorings that were maintained as part of other measurement programs (see Figure 2 for the locations of the moorings).

(i) Barrow Canyon Array

An array of 6 moorings was maintained across the head of Barrow Canyon during 2011 by the Bureau of Ocean Energy Management, Shell, and Conoco Phillips. For a detailed description of the array the reader is referred to Weingartner et al., (2013b). Each mooring contained an upward-facing ADCP and near-bottom MicroCat CTD sensor. After low-passing the velocity records using a 36-hour filter to remove the tidal signal, the velocities were averaged vertically over the depth of the water column. All variables were then subsampled to produce hourly timeseries. Since our study focuses on winter water, it was necessary to consider a broader time period for the Barrow Canyon mooring records than that coincident with the ICESCAPE II cruise. This is because the canyon is situated along the eastern-most pathway of Pacific Water (see Figure 1), which is characterized by swift northeastward flow. Hence the flushing of winter water along this branch is faster than along the other pathways. In order to capture the normal seasonal presence of the winter water at the head of Barrow Canyon, we used the mooring data from May – July 2011. The ADCP velocity data are available for this period for all 6 moorings. However, the Microcat CTD sensor at the offshore-most mooring experienced technical problems in early May, limiting the temporal coverage to 11 days at that site.

(ii) Interior Moorings

Data from three additional moorings were used to identify the flow of winter water in the region between the southern two ICESCAPE hydrographic transects (Figure 2). Detailed information about the moorings, as well as the data availability for the three sites, is available at https://workspace.aoos.org/group/6316/project/56008/files. The western site (Crackerjack) and middle site (Burger) were maintained by Shell, and the eastern site (Klondike) was maintained

by Conoco Phillips. At each of the sites velocity was measured using an upward-facing ADCP, and pressure, temperature, and salinity were measured using ancillary CTD sensors. Unfortunately, only data from 2009-10 are available for the interior moorings. However, since we are considering only time periods that are characterized by relatively steady winds (i.e. no storm events, see below), it is reasonable to use data from the same season during these previous years (similar reasoning applies for including the southern-most CTD transect from ICESCAPE I). The ADCPs on the interior moorings measured the velocity in three bins (surface, middle, and bottom), and the data were similarly low-passed and subsampled to produce daily values. The salinity values at the Klondike site were unrealistically large, hence this timeseries was omitted from our analysis.

(iii) Removing Storm Events

As detailed below in Section 3, the ICESCAPE II cruise occurred during a time when the winds were relatively steady. As such, it was necessary to remove any time periods in the mooring records that were influenced by strong storms. This was accomplished using the hourly-averaged Pt. Barrow weather station wind record in conjunction with the mooring velocity data. In particular, for the Barrow Canyon moorings we used the component of wind and water column velocity along 56 °T (the along-canyon direction), since the two variables are most significantly correlated in this direction (Nobre and Pickart, 2014). The most prevalent wind events are upwelling storms when the winds blow strongly out of the northeast for a period of several days or longer, associated with up-canyon (southwest) flow with a lag of roughly 12 hours. Accordingly, we scrutinized the Barrow Canyon mooring data and Pt. Barrow wind record for the signature of such wind-forced upwelling, and found two events in May 2011 and one in May 2010. These periods were removed from the mooring data. An analogous procedure was applied to the three interior mooring sites, and one upwelling event in both May 2009 and May 2010 were removed from those records.

2.62 Bering Strait

To help interpret the variation in winter water properties in the shipboard data we used timeseries data from mooring A3 in Bering Strait during spring/summer 2011 (see Figure 1 for

the location of the mooring). The instrumentation included a MicroCat and an upward-facing ADCP at 48 m depth. As with the other timeseries data, the records were low-passed then subsampled hourly. Detailed information about the mooring can be found at http://psc.apl.washington.edu/HLD/Bstrait/CruiseReportKhromov2010wEL_verNov11.pdf.

3. Results

3.1 Atmospheric Setting

It is of interest to characterize the atmospheric conditions during which the ICESCAPE program took place. Since this study focuses on the 2011 cruise, we present results from that time period, i.e. 25 June to 29 July, 2011. Throughout the five week cruise the winds were predominantly out of the east/northeast (Figure 3). In fact, the only brief period of westerly winds occurred during the occupation of the BCC transect (Barrow Canyon, Figure 2). The mean wind speed over the domain was 6.6 m/s along 246^{o}T. How does this compare to the typical early summer conditions? Using the NARR data we constructed maps of the mean sea level pressure (SLP) and 10 m winds for the period 2000-2011 (Figure 4, top row). At this time of year there is a signature of the Beaufort High (Moore, 2012) associated with anti-cyclonic winds in the northern Chukchi Sea and Canada Basin. However, there is very little evidence of the Aleutian Low in the Bering Sea and Gulf of Alaska during the summer, which is consistent with the seasonality of this feature (Favorite et al., 1976).

Compared to the 12-year climatology, in summer 2011 the Beaufort High was strong and displaced to the northwest, and there was a well-developed Aleutian Low situated in the northern Bering Sea (Figure 4, middle row). Together, these two centers of action led to enhanced easterly winds in the northern Chukchi Sea. Spall et al. (2014) argue that these winds drove upwelling at the shelfbreak which led to the massive phytoplankton bloom observed at the northern end of transect CSW on the 2011 cruise. The anomaly fields indicate, however, that the very southern portion of the Chukchi shelf and the Bering Strait region experienced weaker winds than normal (Figure 4, bottom row).

To obtain an overall characterization of the winds on the Chukchi shelf we considered a box encompassing the shelf (see Figure 4) and computed the mean wind vector for each of the 12 years corresponding to the early summer period (Figure 5). Consistent with the results of earlier studies (Brugler et al., 2014; Spall et al., 2014) one sees that, in general, the winds in summer have increased over the latter half of the period (with the exception of 2010 when the winds were quite weak). Brugler et al. (2014) attributed this to a combination of a stronger Beaufort High and deeper Aleutian Low (primarily the latter), and this is consistent with the SLP anomaly map of Figure 4 for 2011. In addition to the increased wind speed in recent years, the meridional component has become northerly, as opposed to earlier in the decade when it was mostly southerly.

According to the idealized model study of Winsor and Chapman (2004), the circulation in the Chukchi Sea is most sensitive to easterly winds (relative to the no wind case). For an easterly wind speed of 7.7 m/s their model streamlines veered to the western side of the shelf, and the coastal pathway on the northeast shelf (i.e. the model equivalent of the Alaskan Coastal Current) reversed to the south. In light of the fact that the mean zonal wind speed measured by the ship (Figure 3) was 6 m/s out of the east, this would suggest that the circulation during the 2011 cruise should have been significantly influenced by the wind. However, as seen below, the coastal pathway was quite strong, and the combined transport of the two main flow branches on the eastern shelf was comparable to that measured earlier in the decade under weaker winds (Gong and Pickart, 2015). This apparent discrepancy is resolved by noting that in Winsor and Chapman's (2004) model the winds were applied over the entire domain, and, as seen in Figure 5, according to the NARR the average windspeed over the entire Chukchi Sea was smaller (zonal component of 2 m/s) due to the weak winds in the southern part of the shelf (Figure 4, second row). One should also keep in mind that Winsor and Chapman's (2004) model was idealized (e.g. it was barotropic). In any event, we characterize the winds during the ICESCAPE II cruise as being generally steady and of moderate strength, but not strong enough to reduce the transport of Pacific water in the eastern Chukchi Sea nor cause any flow reversals on the shelf.

372 **3.2 Identification and Characteristics of Winter Water**

373

374 As discussed in the introduction, winter water is formed when surface water freezes and the
375 resulting brine rejection leads to convective overturning of the water column. Consequently, the
376 newly ventilated winter water is close to the freezing point; such water is commonly observed in
377 near-bottom mooring records on the Chukchi shelf during winter (e.g. Weingartner et al., 1998;
378 Woodgate et al., 2005). By the time that the two ICESCAPE surveys took place in June/July the
379 water had warmed somewhat. As such, in this study we define newly ventilated winter water
380 (hereafter referred to simply as winter water) as being colder than -1.6^{o}C with a salinity between
381 31.5 and 33.5.[1] The volumetric T/S plot of Figure 6a demonstrates that this water was the most
382 common water mass present on the Chukchi shelf during the 2011 survey (true as well for 2010,
383 not shown). Roughly 35% of the water on the shelf was colder than -1.6^{o}C. As previously
384 mentioned, this water is of primary importance to the ecosystem of the western Arctic Ocean: it
385 is dense enough to ventilate the upper halocline of the Canada Basin, and its elevated nitrate
386 concentration (Figure 6b) spurs primary production throughout the region.

387

388 We are interested in determining the pathways of the winter water, so for each vertical
389 section in the survey we identified those stations containing winter water that were also located
390 within a well-defined jet as deduced from the absolute geostrophic velocity. For example,
391 consider the Central Channel section (labeled CC in Figure 2), which is shown in Figure 7a
392 (oriented such that the viewer is looking north). One sees that there are three distinct lenses of
393 winter water (middle panel of the figure): one within the channel, one on top of the ridge that
394 forms the eastern side of the channel, and a third narrower lens at the base of the slope leading to
395 the Alaskan coast. The first and third lenses are embedded, respectively, in two poleward jets
396 (right-hand panel of Figure 7a, where the -1.6^{o}C isotherm is marked by the thick black line). The
397 western jet is the well-known Central Channel branch and is associated with downward-sloping
398 isopycnals to the east resulting in a bottom-intensified flow. The eastern jet is the Alaskan
399 Coastal Current (ACC). One sees that at this early point in the summer the ACC is advecting the
400 last vestiges of winter water at depth along with warm Alaskan coastal water in the upper layer

[1] There was no Atlantic water or hyper-saline Pacific winter water (Weingartner et al., 1998) observed on the Chukchi shelf during either ICESCAPE cruise, hence none of the water sampled was saltier than 33.5.

401 (in this snapshot the current is weakly baroclinic). Curiously, the third lens of winter water in the
402 CC section is centered in a region of weak southward flow.
403
404 At the next section to the north (CN in Figure 2), the Central Channel is no longer a
405 topographic feature. Now there are only two lenses of winter water. The first is located on the
406 outer shelf, and much of it is embedded in a poleward jet (Figure 7b). Clearly this is the Central
407 Channel branch after it has emerged from the channel, but it also appears to include a
408 contribution from Herald Canyon that has been diverted eastward along the northern shelf. This
409 is because of the relatively large width of the feature (shown below), and the fact that the inner
410 part of the jet contains substantially warmer water in the upper layer. This suggests a shorter
411 residence time from Bering Strait for that portion of the jet (transporting warm water from the
412 Bering Sea). The second lens of winter water in the CN section straddles the top of the ridge in
413 the middle of the transect. This is the same ridge that was present in the CC section; as seen in
414 Figure 1, the ridge extends to the southwest from Hanna shoal (and contains numerous gaps). As
415 was the case in the CC section, the lens of winter water on the ridge in the CN transect is
416 progressing to the south (the transport is greater here, see below). We believe that this is not a
417 coincidence, and that winter water flows back towards Bering Strait along the ridge. This is
418 further supported by the fact that the same feature was present in the 2010 occupation of CN (not
419 shown). We discuss the origin and fate of this pathway in Section 3.3.
420
421 It is instructive to show two more vertical sections from the 2011 ICESCAPE survey: the
422 CSC transect and the HSSE transect (Figures 7c and 7d, respectively). The former crosses the
423 shelfbreak into the Canada Basin, and one sees that there is a thin layer of winter water
424 extending across the shelf onto the upper-slope. All of this water is progressing eastward,
425 transported by two distinct currents – the shelfbreak jet and a jet on the shelf. The shelfbreak jet
426 is characterized by isopycnals sloping downward offshore which leads to a bottom-intensified
427 flow. This is consistent with the shelfbreak jet observed in the Beaufort Sea at this time of year
428 (i.e. a bottom-intensified flow of winter water, see Spall et al., 2008). However, unlike the
429 Beaufort shelfbreak jet which arises largely from outflow from Barrow Canyon (Pickart et al.,
430 2005), the shelfbreak jet in Figure 7c is being fed from the Herald Canyon outflow (Pickart et
431 al., 2010). The mid-shelf jet at section CSC is likely the continuation of the poleward jet at

section CN. The final section shown (HSSE) extends from Barrow Canyon to Hanna Shoal, and in Figure 7d the viewer is looking southward. We include this transect because modeling studies suggest that the Pacific water emanating from Bering Strait through the Central Channel should flow anti-cyclonically around Hanna Shoal. As seen in Figure 7d, there is indeed a well-defined jet on the shelf advecting winter water to the southwest (although the amount of winter water at this location is small).

3.3 Circulation Diagram and Volume Transports

Using the information from the complete set of vertical sections in Figure 2, together with the mooring data, we now construct a map of winter water circulation on the northeast Chukchi shelf. Figure 8 shows the lateral distribution of potential temperature averaged over the bottom 15 m of the water column (excluding stations with bottom depth deeper than 85 m). Overlaid on this are vectors denoting the transport per unit width associated with the winter water at each CTD station (i.e. water colder than -1.6^{o}C). The reader should keep in mind that these are not true vectors, but instead represent the flow normal to each transect from the absolute geostrophic velocity. (We note that the winter water transport was so small at some of the stations that the vectors are not visible in Figure 8.) At the mooring sites we have plotted the mean near-bottom velocity vectors (true vectors) for the winter water (excluding storms, as explained above). From this figure some clear patterns emerge.

One sees that the coastal pathway is characterized by the warmest temperatures on the shelf. This pathway extends into Barrow Canyon (along the eastern flank of the canyon) and is broadest at the IC section where the bathymetry becomes nearly flat going offshore. Note also that the bottom water on the top of Hanna Shoal is relatively warm. The shoal is thought to be a region of stagnant flow (Martin and Drucker, 1997), although this could not be verified here because the water depth on top of the shoal was too shallow for *Healy's* hull-mounted ADCP to return useful data. Aside from these two regions, the deep portion of the shelf was largely filled with winter water. The anti-cyclonic pathway of this water from Central Channel around Hanna Shoal is clearly evident, providing the first unambiguous observational evidence of this

462 circulation feature predicted by the models. However, close inspection of Figure 8 reveals some
463 unexpected aspects of the circulation not seen in previous numerical simulations.
464
465 Based on this figure we constructed a flow schematic showing the progression of winter
466 water across the shelf (Figure 9a). This circulation diagram is true to the data, with the following
467 caveats. First, although there was no water colder than -1.6°C observed at section IC during the
468 ICESCAPE II cruise, it is safe to assume that, earlier in the season, winter water was advected
469 along the coastal pathway through this section. This is consistent with the fact that the water
470 within the ACC at section IC was the coldest in the entire transect (<0°C), and the fact that
471 winter water was observed at the head of Barrow Canyon earlier in the season in the mooring
472 data. Secondly, at section BCX there is negligibly small transport of winter water in the two
473 pathways identified on this section (see Figure 9b). However, the two jets that were observed on
474 the transect were transporting anomalously cold water (<-1.4°C), which we take to be the
475 leading edge of the winter water along this route. Finally, during the occupation of the CSW
476 section the shelfbreak jet was in the process of spinning back up after a wind-driven flow
477 reversal (see Spall et al., 2014), so the eastward transport of winter water in the jet was
478 somewhat small at this time.
479
480 The flow map of Figure 9a is the first observationally-based depiction of winter water
481 circulation on the northeast Chukchi shelf. The two well-known pathways of Pacific water on
482 the eastern portion of the shelf– the ACC and the Central Channel branch – advect water to the
483 north. The latter is then joined by water that was diverted from Herald Canyon, and together this
484 merged flow approaches Hanna Shoal. However, rather than simply flowing around the northern
485 side of the shoal as predicted by the models, this branch splits and the Pacific water progresses
486 around both sides of the shoal. These two branches subdivide further as the water progresses
487 towards the head of Barrow Canyon. There is also evidence of an offshoot from the Central
488 Channel pathway just north of channel. Thus, there are two means by which winter water feeds
489 Barrow Canyon: (1) a direct coastal route which flows along the eastern flank of the canyon (fed
490 by some water diverted from the Central Channel); and (2) a circuitous pathway that divides into
491 a number of smaller filaments together providing water to both sides of the canyon. The coastal
492 route is swift and the winter water is largely flushed through this pathway by early summer,

493 while the interior route is substantially longer with slower flow speeds feeding Barrow Canyon
494 well into the summer (see also Nobre et al., 2014). Finally, winter water flows to the east in the
495 shelfbreak jet which will ultimately reach the mouth of Barrow Canyon and likely interact with
496 the outflow from the shelf.
497
498 The synoptic volume transports computed along these different flow paths (marked in
499 Figure 9b and listed in Table 1) give a remarkably consistent view. We present the transport of
500 winter water for each section (black numbers), along with the total transport of the flow feature
501 in which the winter water is embedded (red numbers). Starting with the coastal jet, the total
502 transport is the same at sections CC and IC (0.43 Sv and 0.44 Sv, respectively), but, as noted
503 above, there was little to no winter water remaining in this pathway by the time that the
504 ICESCAPE surveys took place. The total transport of shelfbreak jet varied from 0.10 Sv to .28
505 Sv. However, as noted above, the CSW transect was occupied near the end of a period of
506 enhanced easterly winds, so the jet (particularly its upper layer) was still largely reversed at that
507 location (see Spall et al., 2014). Assuming that the undisturbed transport is significantly larger
508 than this, it appears that there was a general diminishment of transport of the jet towards the east.
509 This was true as well for the winter water transport (which on average accounted for
510 approximately 60% of the total transport of the shelfbreak jet).
511
512 The total transport of the mid-shelf flow evolves as follows. Progressing along the Central
513 Channel pathway, the volume flux remains roughly constant as it goes from CC to CSW
514 approaching Hanna Shoal (order 0.5 Sv).[2] East of here, where the flow bifurcates, there is
515 roughly an equal split in transport around the two sides of the shoal. In particular, 42% of the
516 transport progresses anti-cyclonically around the northern side of the shoal, and 58% of the
517 transport progresses cyclonically around the southern side. Encouragingly, the sum of these two
518 branches (eastward transport at HSN + southward transport at CSW = 0.53 Sv) is nearly
519 identical to that approaching the shoal (eastward transport at CSW = 0.51 Sv). As these two
520 branches flow around Hanna Shoal they split again into smaller filaments. On the southern side
521 the split is nearly even in transport (0.16 Sv at CN versus 0.19 Sv at HSS) and roughly conserves

[2] There is an increase in transport where the Herald Canyon branch merges with the Central Channel branch, but keep in mind that the CC section was occupied in 2010.

mass (total of .35 Sv compared to .31 Sv before the split). On the northern side, the transport remains constant from HSN (0.22 Sv) to CSE (0.23 Sv), but then decreases in value at HSSE (.11 Sv). This decrease likely arises because some of the flow is diverted to the outer-shelf or into the shelfbreak jet due to the presence of a small canyon upstream of HSSE. We note that there is a small amount of water (including winter water) flowing southward on the eastern end of this section (not shown), which has also been observed in larger amounts in other hydrographic surveys (R. Pickart, unpublished data). Beyond section HSSE the anti-cyclonic branch splits into two filaments, with most of the transport going into the northern filament.

Importantly, mass is conserved over the locus of the flow branches in Figure 9 (within the uncertainty of the transport measurements), and we can account for the volume flux observed through the head of Barrow Canyon. At section BCH, 0.99 Sv of Pacific water is flowing northward through the canyon, which is approximately equal to the sum of the ACC transport in the coastal route and the transport in the Central Channel branch (together totaling 0.96, using the average value for CC, CN, and CSW). Furthermore, we can make inferences about the partitioning/origin of the flow through the canyon. As seen in Figure 9b, 0.20 Sv is flowing northward on the western flank of the canyon at BCH, and 0.79 Sv is flowing northward on the eastern flank. This implies that the water flowing anti-cyclonically around the northern side of Hanna shoal (order 0.2 Sv) feeds the western flank of Barrow Canyon, while the combination of the water flowing cyclonically around the southern side of Hanna Shoal plus the ACC (which together sum to order 0.8 Sv) feeds the eastern flank. We note that this is consistent with the mean vectors from the Barrow Canyon mooring array which show southeastward flow emanating from south of Hanna Shoal to the eastern side of the canyon (Figure 8).

The transport of winter water on the mid-shelf is partitioned similarly to the full transport of the branches (Figure 9b), although mass doesn't need to be (nor is) conserved over the whole domain because of the seasonal presence of this water mass. As was the case for the full transport, roughly half of the winter water from the Central Channel branch flows on either side of Hanna Shoal (roughly 0.25 Sv approaches the shoal, and 0.13 Sv continues east while 0.13 Sv is diverted south). The difference now is that, in the region where the filaments form, the transport of winter water is quite small. Upstream of here 46% of the total transport (on average)

is due to winter water, which decreases to only 17% in the filaments. This suggests, as noted above, that in the 2011 survey this region was at the leading edge of the winter water, which is consistent with the small amount of water colder than -1.6^{o}C observed flowing north in Barrow Canyon (most of the winter water in the coastal branch had likely passed through the canyon prior to the survey). Later in the season the winter water from the interior pathways around Hanna Shoal should begin draining through the canyon. This is in line with the observation that winter water is prevalent at section BCC during August but not July (Nobre and Pickart, 2014).

3.4 Evolution of Winter Water Properties along the Central Pathway

3.41 In-situ Observations

While all of the winter water on the shelf during the ICESCAPE II cruise was confined to a relatively narrow temperature range (-1.78^{o}C to -1.6^{o}C), the salinity of this water mass displayed substantial variation along the central pathway. This is seen in Figure 10, where we have excluded the 2010 data (to remain synoptic) and have isolated the branch that flows from the Central Channel anti-cyclonically around the north side of Hanna Shoal.[3] One sees that there is an abrupt change in salinity of the winter water starting at the CSC line; i.e., the water becomes markedly fresher. It is of interest to know whether this change was due to variation in the properties of the winter water entering Bering Strait as the season progressed, or the result of local processes on the Chukchi shelf. To answer this we need to know when the water that was measured at each section passed through Bering Strait. The simplest approach is to assume a constant advective speed along the pathway. From the absolute geostrophic velocity, the average speed for the six 2011 sections in Figure 10 is 11.7 ± 2.8 cm/s (varying between 8.1 cm/s at HSSE and 15.6 cm/s at HSN). For reasons explained below, we chose an advective speed of 10.5 cm/s, and Figure 11 shows the mean potential temperature and salinity of the winter water at each section as a function of elapsed time from Bering Strait. One sees that the salinity decreases and the temperature increases for an elapsed time greater than 100 days (i.e.

[3] We have attempted to exclude the portion of the flow that emanates from Herald Canyon by not considering the outer-shelf portions of the sections in question.

downstream of section HSN along the pathway). If this is due to changes in the winter water entering the Chukchi Sea, it means that, later in the season, the winter water flowing through Bering Strait was saltier and colder.

To investigate this we used the timeseries data from mooring A3 in the northern part of Bering Strait in 2011. During the time period from late-December 2010 to early-May 2011, the water entering the strait was at/near the freezing point, with very little variation in temperature (not shown). The salinity, on the other hand, fluctuated quite a bit over this time. Using the chosen advective speed of 10.5 cm/s, this implies that the winter water sampled between sections CN and HSSE in Figure 9 passed through Bering Strait between 20 March and 11 April (indicated by the grey shading in Figure 12). This range of dates of course depends on the advective speed chosen, and, because of the uncertainty in our mean estimate, we considered a range of speeds. However, as seen below in Section 3.42, a choice of 10.5 cm/s leads to the most sensible results, and this value is well within the uncertainty of the calculated mean along the central pathway.

One sees in Figure 12a that there was very little change in temperature of the winter water in Bering Strait over this three week period (ranging from -1.77^{o}C to -1.79^{o}C). The temperatures measured at the six CTD transects, on the other hand, ranged from -1.73^{o}C to -1.62^{o}C (Figure 11). Hence the winter water warmed during its transit along the pathway on the central shelf, which is not surprising (likely due to solar warming as the ice receded and/or lateral mixing with water outside of the pathway). The salinity of the winter water in the strait did vary significantly over the three week period (Figure 12b); however, there was no trend. In particular, the water did not become systematically saltier over this time which would have had to be the case in order to explain the along-pathway variation seen in Figure 11. This implies that there was some means by which the later-arriving winter water was salinized on the Chukchi shelf subsequent to flowing through Bering Strait.

To see this more clearly, we plotted the temperature and salinity of the winter water measured at each section, adjusted back in time to when the water passed through Bering Strait, compared to the mooring timeseries (Figure 13). This shows the degree of warming that took

612 place on the shelf (Figure 13a), indicating that the later-arriving water (after 27 March) warmed
613 less. The salinity comparison reveals that the earlier-arriving water (prior to 27 March) is in line
614 with what was observed at the northern end of the central pathway in Figure 9 (i.e. sections
615 CSC, CSE, and HSSE). That is, the spatial variation in these sections generally follows the
616 temporal variation of the water passing through Bering Strait during this time. However, the
617 salinity at the southern three transects (CN, CSW, and HSN) is significantly larger than the
618 water that flowed through the strait in the latter part of the time period. Hence we need to
619 identify a mechanism that increased the salinity of this later-arriving winter water by 0.2 – 0.3
620 north of Bering Strait. We now argue that freezing and brine rejection, associated with polynya
621 formation, likely modified the winter water that was sampled in the southern part of the pathway
622 during the ICESCAPE II cruise.
623
624 **3.42 Polynya-driven water mass transformation**
625
626 A number of polynyas are observed to form in the Chukchi Sea during the winter and
627 spring. These include the Seward Peninsula Polynya, the Kotzebue Sound Polynya, the Cape
628 Lisburne Polynya, and the Northeast Chukchi Polynya (Stringer and Groves, 1991; Cavalieri and
629 Martin, 1994; Martin et al., 2005). Previous work has estimated the ice production and resulting
630 salt flux into the ocean that occurs in these polynyas (Winsor and Bjork, 2000). We follow this
631 methodology to assess changes in salinity of the winter water as it passed through the southern
632 Chukchi Sea in the early part of summer of 2011. We adopt a Lagrangian approach in which the
633 salt enhancement is estimated for parcels that are initiated at the approximate location of the A3
634 mooring (66.3^{o}N) and transit northwards to the CN line along central pathway. We use 167^{o}W as
635 the meridian along which the parcels travel[4] and consider three different speeds: 10 cm/s, 10.5
636 cm/s, and 11 cm/s (outside of this range, the results are very much at odds with the data). The
637 AMSR-E sea concentration data are used to identify regions along the parcel trajectories where
638 brine rejection occurs, and, as outlined in Section 2.5, the NARR fields are then used to estimate
639 the heat loss that leads to sea ice formation and the resulting salt flux into the water column.

[4] This is the approximate longitude of the pathway. Results are not overly sensitive to this choice, and, due to the other uncertainties in the calculation, it was deemed unnecessary to make the pathway vary with latitude in this part of the domain (the precise pathway is in fact unknown).

In Figure 14 we show the sea ice concentration along 167°W between 66°N (near Bering Strait) to 72°N (the approximate latitude of the CN section along the central pathway) from March to July, 2011. During this period the Chukchi Sea transitions from 100% ice cover to open water. Also shown are the locations of the parcels started at 66.3°N on March 20, April 8, and April 20 with velocities of 10, 10.5 and 11 cm/s for each start date. As one can see, the parcels released on March 20 transit the region under 100% ice cover except for two short periods around April 1 and April 15 when they pass through regions of reduced ice cover near 68°N. This implies minimal salinization of the water, indicating that parcels leaving Bering Strait near that time would not be significantly transformed. This is consistent with Figure 13b. However, the parcels released on April 8 pass through the second of these regions of reduced ice cover during the latter half of April, as well as another region of reduced ice cover in May between 69°N and 71°N, resulting in an extended period of time within a polynya. Finally, the parcels released on April 20 spend the first month of their transit under sea ice before passing into permanent open water later in the season. This suggests that the middle of the three release times (or thereabouts) is most conducive for modification of the winter water in polynyas while re-freezing is still occurring; this is again consistent with figure 13b.

A series of snapshots of the sea ice concentration in the southern Chukchi Sea, from mid-April to early-June, reveals that it is within the Cape Lisburne polynya where the salinization of the winter water likely occurs (Figure 15). In particular, the early parcels (blue symbols) pass by Cape Lisburne before the polynya opens up substantially, and stay north of the region of reduced ice cover as they advect poleward. By contrast, the middle parcels (cyan symbols) first enter the polynya south of Pt. Hope and remain within the area of reduced ice concentration for a prolonged period, staying near the western edge of the polynya. The later-leaving parcels don't reach the polynya until it is subsumed into the region of melt-back expanding from south to north. Hence, the timing of salinization based on the polynya activity is in line with the data (Figure 13b). We now ask, is the degree of salinity enhancement reasonable as well?

To answer this, we estimated the change in salinity along a parcel trajectory as follows. Sea ice production was deemed to occur when the sea ice concentration was less then 100% and the

sea surface temperature was at the freezing point. When these conditions were met, sea ice production was assumed to occur at a rate:

$$P = \frac{Q_{net}}{\rho_{ice} L_h},$$

where P is the ice production rate; Q_{net} is the daily mean net cooling, i.e. the sum of the turbulent (latent and sensible) heat flux and the net longwave radiative flux; ρ_{ice} is the ice density; and L_h is the latent heat of fusion (Cavalieri and Martin, 1994). Following Cavalieri and Martin, 1994, the resulting salt flux is given by:

$$F_s = \rho_{ice} P \left(S_w - S_i \right),$$

where F_s is the salt flux; S_w is the salinity of the ocean water (32.6, based on the observations); and S_i is the salinity of the frazil ice that is given by:

$$S_i = 0.31 S_w .$$

To provide an estimate of the uncertainty in the calculations, cases were considered in which the ice concentration was varied by $\pm 10\%$ with the proviso that ice concentration cannot be higher than 100% or lower than 0%. The resulting salt flux was assumed to be mixed through the volume of open water at that particular grid point, assuming a constant depth of 40m (typical shelf depth along the pathway), to generate a daily change in salinity. The net change in salinity along the parcel trajectories was then calculated as the sum of these daily changes. In this calculation we do not consider the effect of heating of the sea surface by the net shortwave radiative or turbulent heat flux. The impact of this surface warming is implicitly taken into effect by restricting the generation of the salt flux to conditions where the sea surface temperature is at the freezing point.

The estimated net change in the salinity of the winter water progressing northward along the central pathway from the Bering Strait mooring site to the CN section is shown in Figure 16 for a range of start dates from March 20 to April 23, 2011. There is an overall trend for the salinization to increase for parcels leaving between late-March and early-April, before decreasing the latter half of April. This is expected based on figures 14 and 15, i.e. due to the opening of the Cape Lisburne polynya, followed by the melt-back on the southern shelf. Note that the start date

for maximum salinization is earlier for the slower moving parcels due to the longer time it takes these parcels to reach the location of the polynya. Also, the magnitude of the change in salinity is larger for the slower moving parcels; this is the result of the additional time that they spend in the regions of reduced ice cover.

Based on these results and the analysis of Section 3.41, a parcel velocity of 10.5 cm/s provides the best fit to the data. For this choice, the largest change in salinity is ~0.25 for parcels leaving the Bering Strait mooring site around April 8. Due to the uncertainty in the actual advective speed (which surely varied over the course of the central pathway), and in light the various assumptions made in the salt flux calculation, the agreement with figure 13b is quite good. It suggests that we have correctly identified the cause of the increased salinity of the winter water on the three upstream ICESCAPE II transects. This is also consistent with the slightly colder temperature observed on these transects, indicative of more recent convective overturning. We note that the integrated effect of changing the ice cover by +/- 10% along this trajectory results in an approximate 10% uncertainty in the salinity change. A similar uncertainty is expected to occur as a result of biases in the air-sea heat fluxes. The results are also sensitive to the vicinity of the trajectories to the location of the Cape Lisburne polynyas, which of course is not precisely known.

It is worth noting that longwave cooling played a major role in the salinization of the winter water in the southern Chukchi Sea in 2011. In Figure 17 we have plotted the relative contributions of the longwave radiative and turbulent heat fluxes to the change in salinity along 167^{o}W for a parcel velocity of 10.5 cm/s as a function of start date. (Other choices for parcel velocity resulted in similar results.) For early start dates, the turbulent heat flux makes the largest contribution to the total change in salinity. However, after early-April the contribution from the longwave radiative flux dominates. The cooling due to the turbulent heat fluxes is highly episodic and is typically associated with cold air outbreaks where there is a large temperature difference between the atmosphere and the ocean (Renfrew et al., 2002a). The longwave cooling, on the other hand, is typically lower in magnitude but more continuous in time (Renfrew et al., 2002b; Morales Maqueda et al., 2004). The transition in Figure 17 can therefore be understood as being the result of the reduction in the air-sea temperature contrast that occurs as the region warms in

April and May, as well as the more steady nature of the radiative cooling. Recall from figure 14 that the salinization for parcels leaving in early-April (i.e. the best fit to the data) occurred during two distinct periods. The first period of brine rejection was dominated by cooling due to the turbulent heat fluxes, while that during the second period was driven mainly by longwave cooling.

4. Summary and Discussion

The ICESCAPE hydrographic and velocity data, together with contemporaneous mooring data from other programs, have allowed us to construct the most complete circulation diagram to date of the northeast Chukchi shelf during the early-summer time period when newly-ventilated winter water is progressing poleward. The observations suggest that as the Central Channel branch approaches Hanna Shoal it bifurcates and flows around both sides of shoal before dividing into smaller filaments that enter Barrow Canyon. Encouragingly, mass is conserved in this scheme: approximately 1 Sv flows into the northeast part of the shelf via the coastal pathway (the Alaskan Coastal Current, ACC) and the Central Channel pathway, and an equal amount exits through the head of Barrow Canyon. It appears that the branch circulating anti-cyclonically around the northern side of Hanna Shoal feeds the western flank of the canyon, while the branch passing on the south side of the shoal, together with the ACC, feed the eastern flank.

While all of the winter water in the 2011 ICESCAPE survey was relatively close to the freezing point, its salinity varied. In particular, the winter water sampled in the upstream portion of the central pathway was saltier than that measured farther downstream. Mooring timeseries in Bering Strait indicated that this pattern was not due to variation of the inflowing winter water from the Bering Sea. We attributed the increase in salinity to transformation of the water within the Chukchi Sea, as it passed along the western side of the Cape Lisburne polynya in early May. Applying a sea-ice formation / brine rejection algorithm in a Lagrangian framework, the predicted increase in salinity – and its timing – was on par to that measured in the ICESCAPE II survey.

Our results have raised additional questions, and, at the same time, may offer some clues regarding different aspects of the ecosystem of the Chukchi Sea. The first question is, what causes the bifurcation of the flow impinging on Hanna Shoal, which is not seen in the models. One possibility is the presence of a canyon to the east of the HSN line (this can be seen as an incursion of the isobaths in Figure 2, including the 50 m isobath). To first order the flow wants to follow the topography, which means it should be deflected to the south here which may cause it to recirculate to the west of the shoal. Such small scale topographic features may not be present in the models. As noted earlier, another such small canyon is located to the north of the HSSE line, which could cause some of the flow to divert from the shelf in that area. Canyons such as these offer the chance for interaction between the shelfbreak jet and the circulation on the outer shelf. Another question (for which we don't have an answer) is, why does the flow on either side of Hanna Shoal break up into smaller filaments? Here again topography may be a contributing factor. For example, several distinct jets were observed crossing the corrugated ridge between Hanna and Herald Shoals. It could be that the water is seeking gaps in the ridge through which to flow to the east. Stability of the flow may be another factor. It should also be remembered that the wind was mostly from the east during the ICESCAPE II survey and this would tend to decelerate the eastward flow on the shelf, which perhaps played a role. Overall, our study downplays the notion that the flow of Pacific-origin water on the Chukchi shelf is confined to three main branches.

The data presented here highlight the fact that there is a fast coastal pathway (which was nearly void of winter water by the time the ICESCAPE surveys took place) and a set of slower pathways on the interior shelf. This is potentially of importance for the distribution of nutrients and the subsequent growth of phytoplankton on the shelf. As shown above, the winter water is high in nitrate, and a slow residence time means that such nutrients remain on the shelf as the ice retreats and more sunlight penetrates the water column. Of note is the fact that there is a convergence of several slow pathways in the region south of Hanna Shoal. This is the area where enhanced numbers of walrus have been observed (Hannay et al., 2013). Prolonged primary production and carbon export to the bottom is conducive for a rich benthic habitat which should attract walrus. Similarly, our results imply that much of the water encircling Hanna Shoal drains into the western side of the Barrow Canyon, and this location is characterized by extraordinarily

high levels of benthic biomass (Grebmeier, 2012). A sustained supply of winter water to this region could help support this "hot spot".

Finally, there are strong ramifications to the notion that brine rejection can further transform the winter water flowing poleward in the central pathway. Salinization of winter water on the Chukchi shelf has been documented previously for the coastal pathway (e.g. Weingartner et al., 1998; Itoh et al., 2002). Our results suggest that this can happen for the water in the slower pathways as well. The convective overturning that results from the brine rejection will likely reach the bottom (since the Chukchi shelf is so shallow) which will stir regenerated nutrients from the sediments into the water column (there is evidence of this; R. Pickart, unpublished data). In turn, levels of primary production on the Chukchi shelf could be enhanced because the water has such a long residence time (compared to the swift coastal current that advects the nutrients quickly into the basin). It remains to be determined if such brine rejection in the central pathway occurs on a regular basis.

Acknowledgements

The authors are indebted to the officers and crew of the USCGC *Healy*, whose hard work and dedication led to the success of the ICESCAPE field program. We thank Jules Hummon for her assistance in the processing and quality control of the vessel-mounted ADCP data. The Ocean Data Facility of the Scripps Institution of Oceanography processed and calibrated the CTD data and ran the nutrient samples. Special thanks are given to Scott Hiller for maintaining the CTD system, Jim Swift for overseeing the CTD operation, and Kevin Arrigo for guiding the overall ICESCAPE program. RP, FB, and CN were funded by the Ocean Biology and Biogeochemistry Program and the Cryosphere Science Program of the National Aeronautic and Space Administration under Award NNX10AF42G (RSP;KRA). GWKM was supported by the Natural Sciences and Engineering Research Council of Canada. TW was supported by the Department of Interior's Bureau of Ocean Energy Management under Cooperative Agreement No. M12AC00008. CM acknowledges the National Oceanography Centre / Woods Hole Oceanographic Institution exchange program, as well as N. Penny Holliday and Harry Bryden for support. ConocoPhillips provided the current meter data from the Klondike site and Shell

822 Exploration & Production Company, provided the current meter data from Crackerjack and
823 Burger sites. These data are available at
824 https://workspace.aoos.org/group/6316/project/56008/files,
825

826 **References**

827

828 Aagaard, K., L.K. Coachman and E.C. Carmak, 1981. On the halocline of the Arctic Ocean.
829 *Deep-Sea Research*, **28**, 529-545.
830 Aagaard, K. and A.T. Roach, 1990. Arctic ocean-shelf exchange: measurements in Barrow
831 Canyon. *Journal of Geophysical Research*, **95**, 18,163-18,175.
832 Armstrong, F., C.R. Stearns, and J. Strickland, 1967. The measurement of upwelling and
833 subsequent biological process by means of the Technicon Autoanalyzer® and associated
834 equipment. *Deep-Sea Research*,**14**, 381–389. doi:10.1016/0011- 7471(67)90082-4
835 Arrigo, K.R, D.K. Perovich, R.S. Pickart, and 28 co-authors, 2012. Massive phytoplankton
836 blooms under Arctic sea ice. *Science*, **336**, 1408.
837 Brugler, E.T., R.S. Pickart, G.W.K. Moore, S. Roberts, T.J. Weingartner, and H. Statscewich,
838 2014. Seasonal to Interannual Variability of the Pacific Water Boundary Current in the
839 Beaufort Sea. *Progress in Oceanography*, **127**, 1-20,
840 http://dx.doi.org/10.1016/j.pocean.2014.05.002
841 Cavalieri, D.J., Crawford, J.P., Drinkwater, M.R., Eppler, D.T., Farmer, L.D., Jentz, R.R. and
842 Wackerman, C.C., 1991. Aircraft active and passive microwave validation of sea ice
843 concentration from the Defense Meteorological Satellite Program special sensor microwave
844 imager. *Journal of Geophysical Research,* **96**, doi: 10.1029/91JC02335. issn: 0148-0227.
845 Cavalieri, D.J., and S. Martin, 1994. The contribution of Alaskan, Siberian, and Canadian
846 coastal polynyas to the cold halocline of the Arctic Ocean. *Journal of Geophysical*
847 *Research,* **99**, 18,343-18,362.
848 DeCosmo, J., Katsaros, K.B., Smith, S.D., Anderson, R.J., Oost, W.A., Bumke, K. and
849 Chadwick, H., 1996. Air-sea exchange of water vapor and sensible heat: The humidity
850 exchange over the sea (HEXOS) results, *Journal of Geophysical Research-Oceans*,
851 **101**(C5), 12001-12016.

852 Favorite, F., A. J. Dodimead, and K. Nasu, 1976. Oceanography of the subarctic Pacific region,
853 1962–72. *Bull. Int. North Pacific Fish. Comm.*, **33**, 1-187.
854 Gong, D. and R.S. Pickart, 2015. Summertime Circulation in the Eastern Chukchi Sea. *Deep-Sea*
855 *Research II*, accepted.
856 Grebmeier, J.M., 2012. Shifting patterns of life in the Pacific Arctic and Sub-Arctic seas. *Ann*
857 *Rev Mar Sci* **4**, 63-78.
858 Hannay, D. E., J. Delarue, X. Mouy, B. S. Martin, D. Leary, J. N. Oswald, J. Vallarta, 2013.
859 Marine mammal acoustic detections in the northeastern Chukchi Sea, September 2007–July
860 2011. *Continental Shelf Research*, **67**, 127-146.
861 Hill, V., G. Cota, and D. Stockwell, 2005. Spring and summer phytoplankton communities in the
862 Chukchi and Eastern Beaufort Seas, *Deep Sea Research II*, **52**, 3369-3385.
863 Itoh, M., K. Shimada, T. Kamoshida, F. McLaughlin, E.C. Carmack, and S. Nishino, 2012.
864 Interannual variability of PWW in flow through Barrow Canyon from 2000 to 2006,
865 *Journal of Oceanography*, doi: 10.1007/s10872-012-0120-1.
866 Itoh, M., R.S. Pickart, T. Kikuchi, Y. Fukamachi, K. I. Ohshima, D. Simizu, K. R. Arrigo, S.
867 Vagle, J. He, C. Ashjian, J. T. Mathis, S. Nishino, C. Nobre, 2015. Water properties, heat
868 and volume fluxes of Pacific water in Barrow Canyon during summer 2010. *Deep-Sea*
869 *Research I*, accepted.
870 Kadko, D., R.S. Pickart, and J. Mathis, 2008. Age characteristics of a shelf-break eddy in the
871 western Arctic Ocean and implications for shelf-basin exchange. *Journal of Geophysical*
872 *Research*, **113**, C02018, doi:10.1029/2007JC004429.
873 Lowry, K.E., R.S. Pickart, M. Mills, Z. W. Brown, G. L. van Dijken, N. Bates, and K. Arrigo,
874 2015. The influence of winter water on phytoplankton 1 blooms in the Chukchi Sea. *Deep-*
875 *Sea Research II*, accepted.
876 Martin, S., and R. Drucke, 1997. The effect of possible Taylor columns on the summer sea ice in
877 the Chukchi Sea. *Journal of Geophysical Research* **102**, 10473–10482.
878 Martin, S., R. Drucker, R. Kwok, B. Holt, 2005. Improvements in the estimates of ice thickness
879 and production in the Chukchi Sea polynyas derived from AMSR-E, *Geophysical Research*
880 *Letters*, **32**(5).

881 Mathis, J.T., R.S. Pickart, D.A. Hansell, D. Kadko, and N.R. Bates, 2007. Eddy transport of
882 organic carbon and nutrients from the Chukchi shelf into the deep Arctic basin. *Journal of*
883 *Geophysical Research*, **112**, c05011, doi:10.1029/2006JC003899.

884 Mesinger, F., and 18 co-authors, 2006. North American regional reanalysis, *Bulletin of the*
885 *American Meteorological Society*, **87**(3), 343+.

886 Mills, M.M, Z.W. Brown, K.E. Lowry, G.L. van Dijken, S. Becker, S. Pal, C. Benitez-Nelson,
887 A.L. Strong, J.H. Swift, R.S. Pickart, and K.R. Arrigo, 2015. Impacts of low phytoplankton
888 NO3-:PO43-utilization ratios over the Chukchi Shelf, Arctic Ocean. *Deep-Sea Research II*,
889 accepted.

890 Moore, G.W.K., 2012. Decadal variability and a recent amplification of the summer Beaufort
891 Sea High. *Geophysical Research Letters*, **39**, L10 807, doi:10.1029/2012GL051 570.

892 Moore, G.W.K., R.S. Pickart, I.A. Renfrew, and K. Våge, 2014.What causes the location of the
893 air-sea heat flux maximum over the Labrador Sea? *Geophysical Research Letters*, **41**, 3628-
894 3635. DOI: 10.1002/2014GL059940

895 Morales Maqueda, M. A., A.J. Willmott, and N.R.T. Biggs, 2004. Polynya Dynamics: a Review
896 of Observations and Modeling. *Reviews of Geophysics*, **42**(1), RG1004.

897 Nobre, C. and R.S. Pickart, 2014. Evolution of Water Masses in Barrow Canyon during
898 Summer/Fall: First Results from the DBO International Transects 2010-13. *Eos Trans.*
899 *AGU*, abstract 13357.

900 Padman, L. and S. Erofeeva, 2004. A barotropic inverse tidal model for the Arctic Ocean.
901 *Geophysical Research Letters*, **31**, DOI: 10.1029/2003GL019003.

902 Panteleev, G., D. A. Nechaev, A. Proshutinsky, R. Woodgate, and J. Zhang, 2010.
903 Reconstruction and analysis of the Chukchi Sea circulation in 1990-1991. *Journal of*
904 *Geophysical Research*, **115**, C08023, doi:10.1029/2009JC005453.

905 Paquette, R. G. and R. H. Bourke, 1974. Observations on the coastal current of Arctic Alaska.
906 *Journal of Marine Research*, **32**, 195-207.

907 Pickart, R. S., T. J. Weingartner, S. Zimmermann, D. J. Torres, and L. J. Pratt, 2005. Flow of
908 winter-transformed Pacific water into the western Arctic. *Deep-Sea Research II,* **52**, 3175-
909 3198.

910 Pickart, R.S., L.J. Pratt, D.J. Torres, T.E. Whitledge, A.Y. Proshutinsky, K. Aagaard, T.A.
911 Agnew, G.W.K. Moore, and H.J. Dail, 2010. Evolution and dynamics of the flow through
912 Herald Canyon in the Western Chukchi Sea. *Deep-Sea Research II*, **57**, 5-26.
913 doi:10.1016/j.dsr2.2009.08.002.

914 Renfrew, I. A., G. W. K. Moore, P. S. Guest, and K. Bumke, 2002a. A comparison of surface
915 layer and surface turbulent flux observations over the Labrador Sea with ECMWF analyses
916 and NCEP reanalyses, *Journal of Physical Oceanography*, **32**(2), 383-400.
917 Renfrew, I. A., J. C. King, and T. Markus, 2002b. Coastal polynyas in the southern Weddell Sea:
918 Variability of the surface energy budget, *Journal of Geophysical Research*, **107**(C6), 16-11-
919 16-22.
920 Renfrew, I. A., S. D. Outten, and G. W. K. Moore, 2009. A comparison of aircraft-based surface-
921 layer observations over Denmark Strait and the Irminger Sea with meteorological analyses
922 and QuikSCAT winds, *Quarterly Journal of the Royal Meteorological Society*, **135**(645),
923 2046-2066.
924 Smith, S. D., 1988. Coefficients for sea-surface wind stress, heat-flux, and wind profiles as a
925 function of wind-speed and temperature, *Journal of Geophysical Research-Oceans*,
926 **93**(C12), 15467-15472.
927 Spall, M.A., 2007. Circulation and water mass transformation in a model of the Chukchi Sea.
928 *Journal of Geophysical Research*, **112**, C05025, doi:10.1029/2005JC003364.
929 Spall, M.A., R.S. Pickart, P.S. Fratantoni, and A.J. Plueddemann, 2008. Western Arctic
930 shelfbreak eddies: Formation and transport. *Journal of Physical Oceanography*, **38**, 1644-
931 1668.
932 Spall, M.A., R.S. Pickart, E.T. Brugler, G.W.K Moore, L. Thomas, K.R. Arrigo. Role of
933 Shelfbreak Upwelling in the Formation of a Massive Under-ice Bloom in the Chukchi Sea.
934 *Deep Sea Research II*, **105**, 17-29.
935 Spreen, G., L. Kaleschke, and G. Heygster, 2008. Sea ice remote sensing using AMSR-E 89-
936 GHz channels, *Journal of Geophysical Research: Oceans*, **113**(C2), C02S03.
937 Stringer, W. J., and J. E. Groves, 1991. Location and areal extent of polynyas in the Bering and
938 Chukchi Seas, *Arctic*, **44**, 164-171.
939 Walsh, J. E., W. L. Chapman, and D. H. Portis, 2009. Arctic Cloud Fraction and Radiative
940 Fluxes in Atmospheric Reanalyses, *Journal of Climate*, **22**(9), 2316-2334.
941 Weingartner, T.J., D.J. Cavalieri, K. Aagaard, and Y. Sasaki, 1998. Circulation, dense water
942 formation, and outflow on the northeast Chukchi shelf. *Journal of Geophysical Research*,
943 **103**, 7647-7661.

944 Weingartner, T., K. Aagaard, R. Woodgate, S. Danielson, Y. Sasaki, and D. Cavalieri, 2005.
945 Circulation on the north central Chukchi Sea shelf. *Deep-Sea Research II*, **52**, 3150-3174.

946 Weingartner, T.K., E. Dobbins, S. Danielson, P. Winsor R. Potter, H. Statscewich, 2013a.
947 Hydrographic variability over the northeastern Chukchi Sea shelf in summer-fall 2008–
948 2010. *Continental Shelf Research*, **67**, 5-22.

949 Weingartner, T., P. Winsor, R. Potter, H. Statscewich, E. Dobbins, 2013b. Final Report:
950 Application of High Frequency Radar to Potential Hydrocarbon Development Areas in the
951 Northeast Chukchi Sea, BOEM Contract No: M09AC15207, 165 p. April, 2013.

952 Winsor, P., and G. Bjork, 2000. Polynya activity in the Arctic Ocean from 1958 to 1997, *Journal*
953 *of Geophysical Research-Oceans*, **105**(C4), 8789-8803.

954 Winsor, P., D.C. Chapman, 2004. Pathways of Pacific water across the Chukchi Sea: A numerial
955 model study. *Journal of Geophysical Research*, **109**, C03002, doi:10.1029/2003JC001962.

956 Woodgate, R.A., K. Aagaard, T.J. Weingartner, 2005. A year in the physical oceanography of
957 the Chukchi Sea: Moored measurements from autumn 1990-1991. *Deep-Sea Research II*,
958 **52**, 3116-3149.

959
960
961
962
963
964
965
966
967
968
969
970
971
972
973
974
975
976

	Mid-Shelf Jet		Coastal Jet		Reversed Flow		Shelfbreak Jet	
	Total	*winter water*	Total	winter water	Total	winter water	Total	winter water
Central Channel (CC)	*.44*	*.22*	.43	.08	-.02	-.01	_	_
Chukchi North (CN)	*.60*	*.27*	_	_	-.16	-.06	_	_
Chukchi Shelfbreak West (CSW)	*.51*	*.24*	_	_	-.31	-.13	.10	.06
Hanna Shoal North (HSN)	*.22*	*.13*	_	_	-.03	-.02	.28	.23
Chukchi Shelfbreak Central (CSC)	*.26*	*.12*	_	_	_	_	.15	.10
Chukchi Shelfbreak East (CSE)	*.23*	*.08*	_	_	_	_	.17	.04
Hanna Shoal Southeast (HSSE)	*.11*	*.02*	_	_	_	_	_	_
Barrow Canyon Head Extension (BCX)	*.18*	*.01*	_	_	_	_	_	_
Hanna Shoal South (HSS)	_	_	_	_	-1.9	-.2	_	_
Icy Cape (IC)	_	_	.44	_	_	_	_	_
Barrow Canyon Head (BCH)	*.20*	*.03*	.79	_	_	_	_	_

977

978 Table 1. Volume transport (in Sverdrups) for the different flow paths associated with the vertical sections
979 in the ICESCAPE II survey. Positive transports are poleward. For each section the total transport is
980 listed along with the transport of winter water. See text for details.

981

982

983

984

985

Figure Captions

Figure 1: Schematic of the circulation of Pacific water in the Chukchi Sea, prior to this study. Place names are listed along with the location of the Bering Strait mooring A3 (black star).

Figure 2: Locations of the shipboard measurements and moorings used in the study. See the legends for details. The US/Russian convention line is plotted.

Figure 3: Wind vectors measured from *Healy* at each of the CTD station locations. The location of the Pt. Barrow weather station is indicated by the star.

Figure 4: NARR fields averaged over the time period of the ICESCAPE II cruise, 25 June –29 July. The left-hand panels are sea level pressure (color and contours, mb) and 10 m wind vectors. The right-hand panels are 10 m wind speed (color) and 10 m wind vectors. Top row: mean conditions for 2000-11. Middle row: Conditions during 2011. Bottom row: Anomaly (2011 – climatology). The black box in the lower right-hand panel marks the region over which the mean winds were computed (see the text and Figure 5).

Figure 5: Mean 10 m wind vectors for the Chukchi Sea from NARR (within the box shown in Figure 4) over the time period of the ICESCAPE II cruise, 25 June –29 July, shown for each year from 2000-11.

Figure 6: (a) Volumetric T/S diagram using the CTD data from the ICESCAPE II cruise. For each bin corresponding to 0.05^{o}C in temperature and 0.05 in salinity, the number of observations (in log counts) is colored. The thick black lines mark the boundary between the water masses. WW = newly ventilated winter water; RWW = remnant winter water; BSW = Bering Sea Water; ESMW = early season melt water. The thin dashed line is the freezing line. (b) Scatter plot of the bottle data in T/S space where the nitrate concentration is colored (μmol/kg).

Figure 7: Vertical property sections for selected transects (indicated by red in the left-hand panels). The middle panels show potential temperature (color) overlain by salinity. The right-hand panels show absolute geostrophic velocity (color, where positive velocities are out of the page) overlain by the -1.6^{o}C isotherm (thick black line).

Figure 8: Average potential temperature (color) in the bottom 15 m of the water column at each station whose bottom depth is shallower than 85m. The vectors at the station sites are the transport per unit width of the winter water. The vectors at the mooring sites are the near-bottom velocities (see the legend).

Figure 9: (a) Winter water flow pathways deduced from the data. (b) Volume transports of the pathways. The red numbers are the total transport and the black numbers are the winter water transport. The station locations are marked by the dots.

Figure 10: Average salinity (color) of the winter water for the stations comprising the central pathway around the north side of Hanna Shoal. The vectors denote transport per unit width of the winter water (from Figure 8).

Figure 11: Average salinity and potential temperature of the winter water along the central pathway of Figure 10, plotted versus elapsed time from Bering Strait (see text for details).

Figure 12: Timeseries of temperature (top panel) and salinity (bottom panel) for mooring A3 in Bering Strait (see Figure 1 for the location of the mooring). The grey shading denotes the time period when the winter water, sampled at the sections in Figure 11 along the central pathway, passed through the strait.

Figure 13: Zoomed-in view of the timeseries of temperature (top panel) and salinity (bottom panel) from Figure 12. The green circles denote the properties of the winter water measured along the central pathway at the sections in Figure 11, adjusted for when the water passed through Bering Strait (see text for details).

Figure 14: Time-latitude variation of sea ice concentration (%) from the AMSR-E along 167°W during March -July 2011. Also shown are the daily location of parcels starting at 66.3°N on March 20 (blue symbols), April 8 (maroon symbols) and April 20 (black symbols). Locations are shown for parcel velocities of 10 cm/s ('+'), 10.5 cm/s ('o') and 11 cm/s ('x').

Figure 15: AMSR-E sea ice concentration (%) on: (a) April 15, (b) May 1, (c) May 15, and (d) June 1 2011. Also shown are the locations of parcels starting at 66.3°N on March 20 (blue symbols), April 8 (maroon symbols), and April 20 (black symbols) and travelling along 167°W. Locations are shown for parcel velocities of 10 cm/s ('+'), 10.5 cm/s ('o') and 11 cm/s ('x').

Figure 16: Change in salinity along 167°W for parcels starting at 66.3°N and ending at 72°N as a function of start date in March/April 2011. Changes in salinity are shown for parcel velocities of 10 cm/s, 10.5 cm/s and 11 cm/s. Error bars indicate the change in salinity resulting from a +/- 10% change in ice cover along the trajectory of the parcels.

Figure 17: Contribution of the longwave radiative flux (blue curve) and turbulent heat flux (red curve) to the total change in salinity (black curve) along 167°W for parcels with a velocity of 10.5 cm/s starting at 66.3°N and ending at 72°N as a function of start date in March/April 2011.

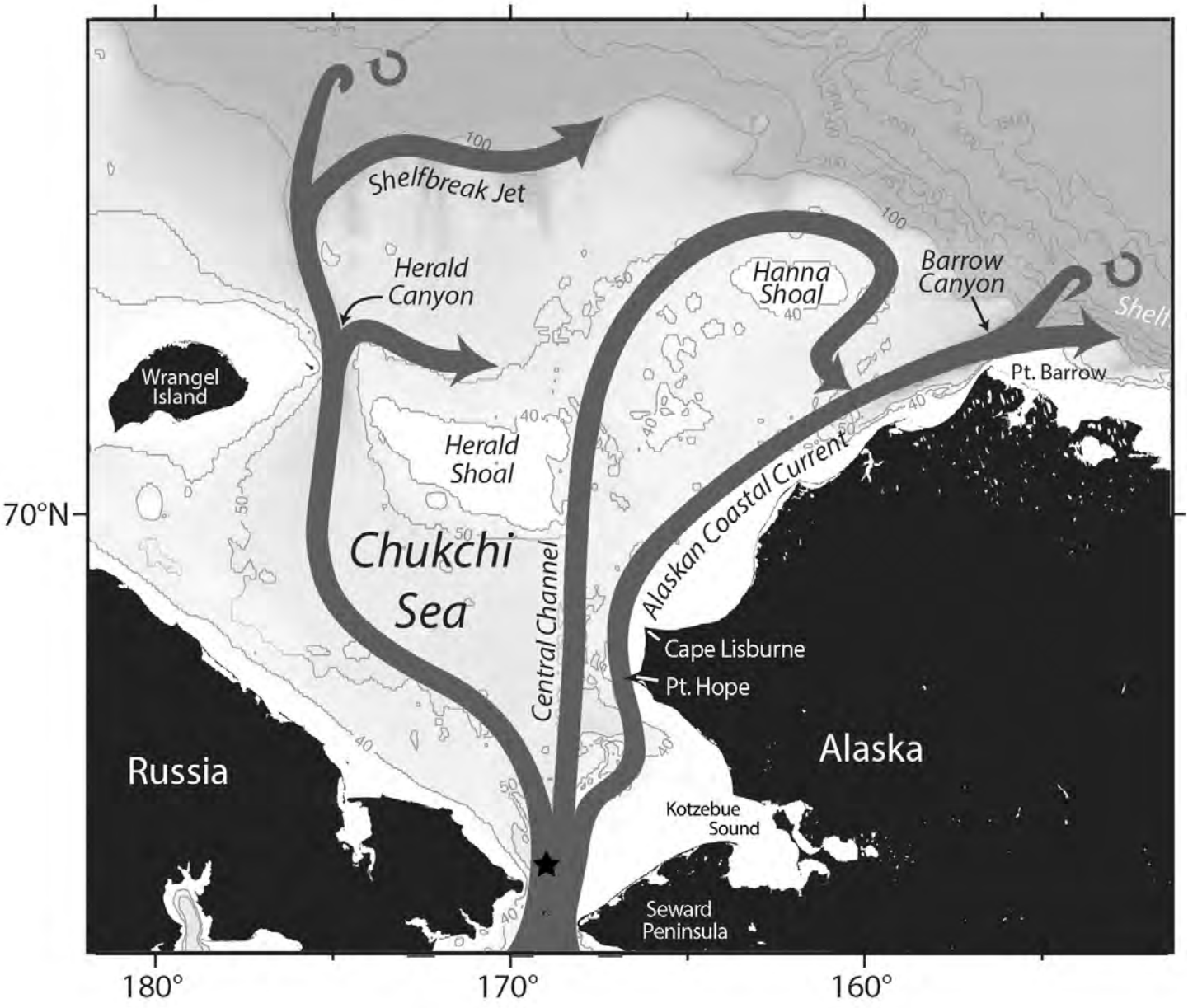

Figure 1: Schematic of the circulation of Pacific water in the Chukchi Sea, prior to this study. Place names are listed along with the location of the Bering Strait mooring A3 (black star).

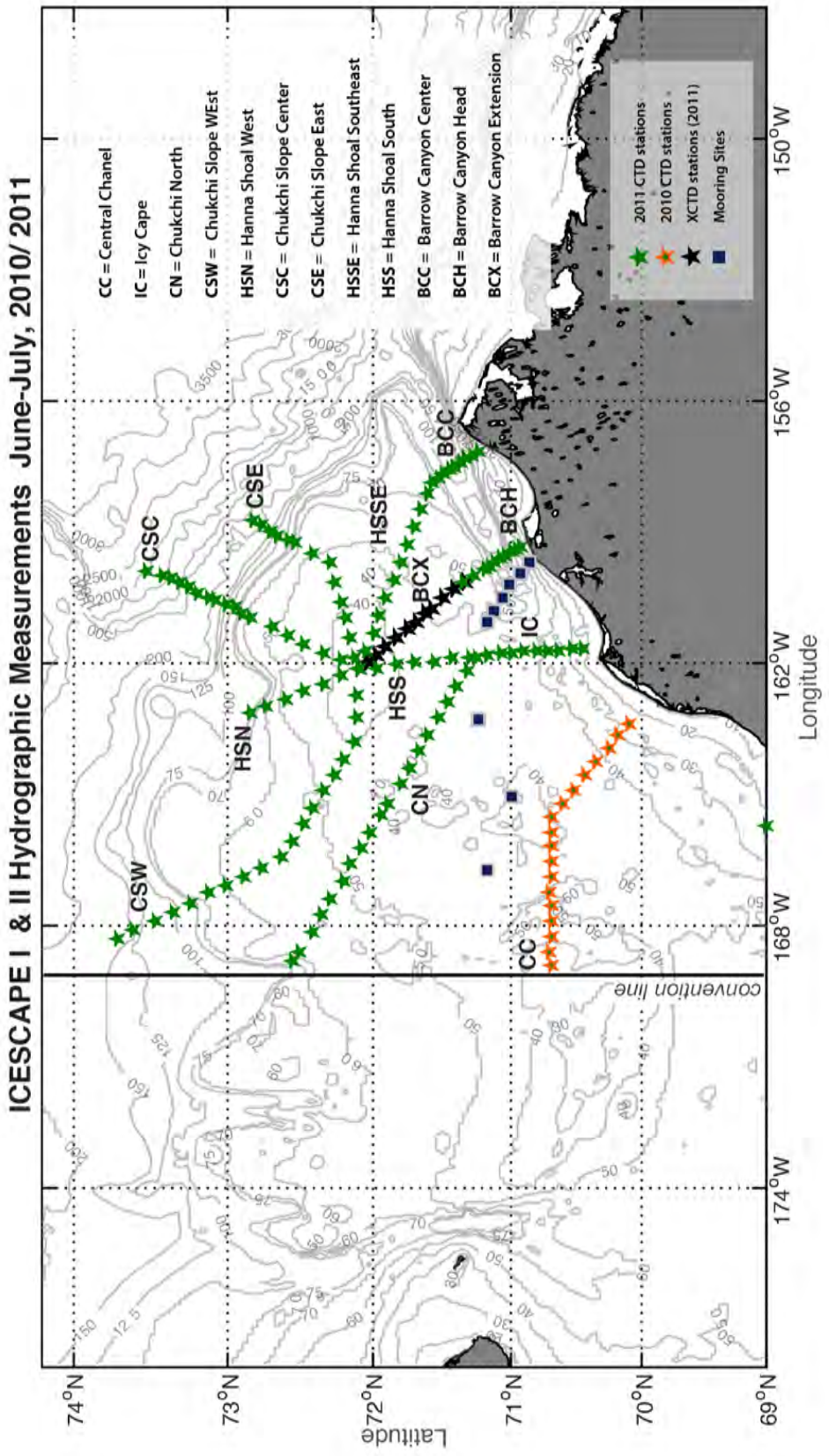

Figure 2: Locations of the shipboard measurements and moorings used in the study. See the legends for details. The US/Russian convention line is plotted.

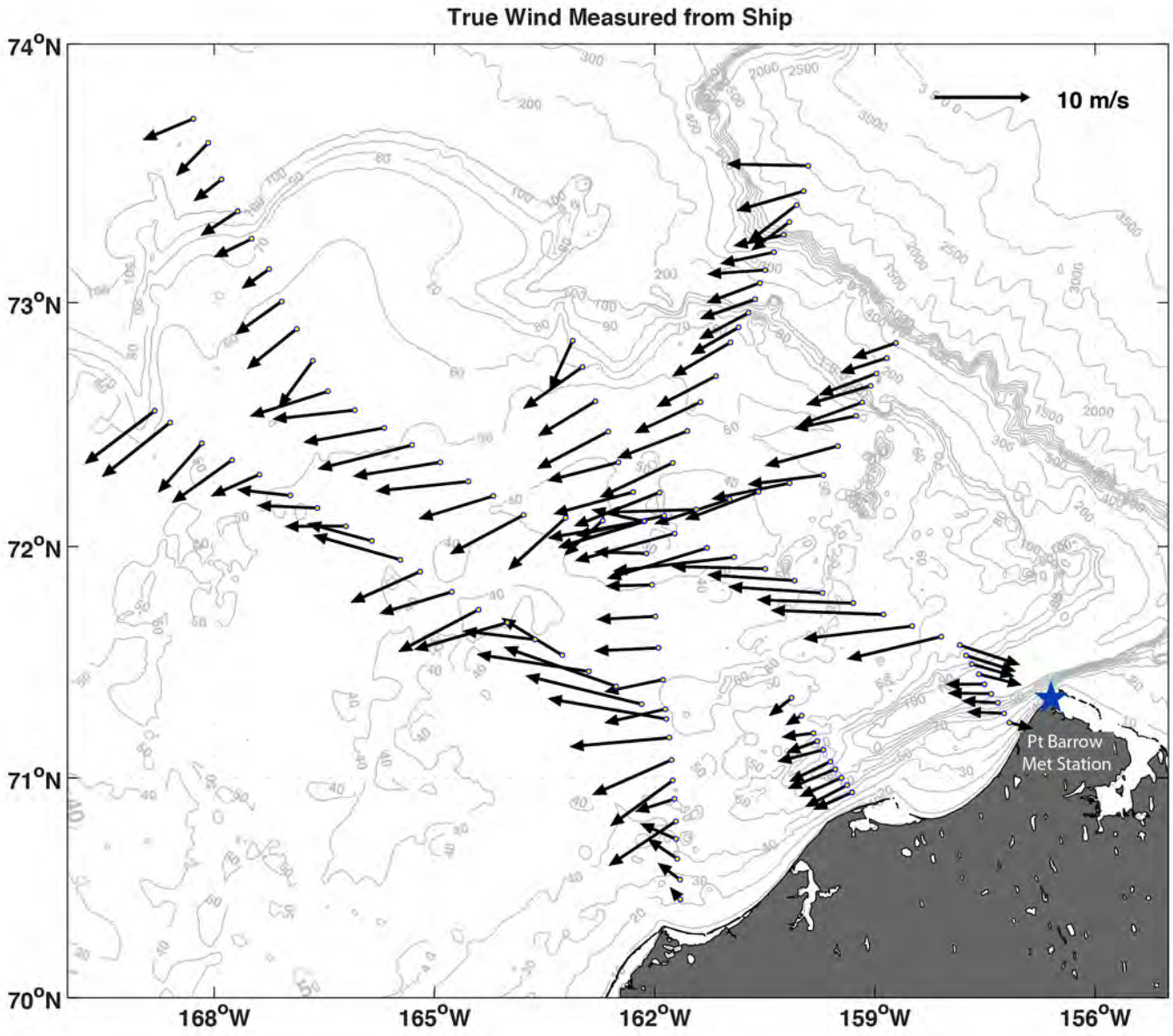

Figure 3: Wind vectors measured from the Healy at each of the CTD station locations. The location of the Pt. Barrow weather station is indicated by the star.

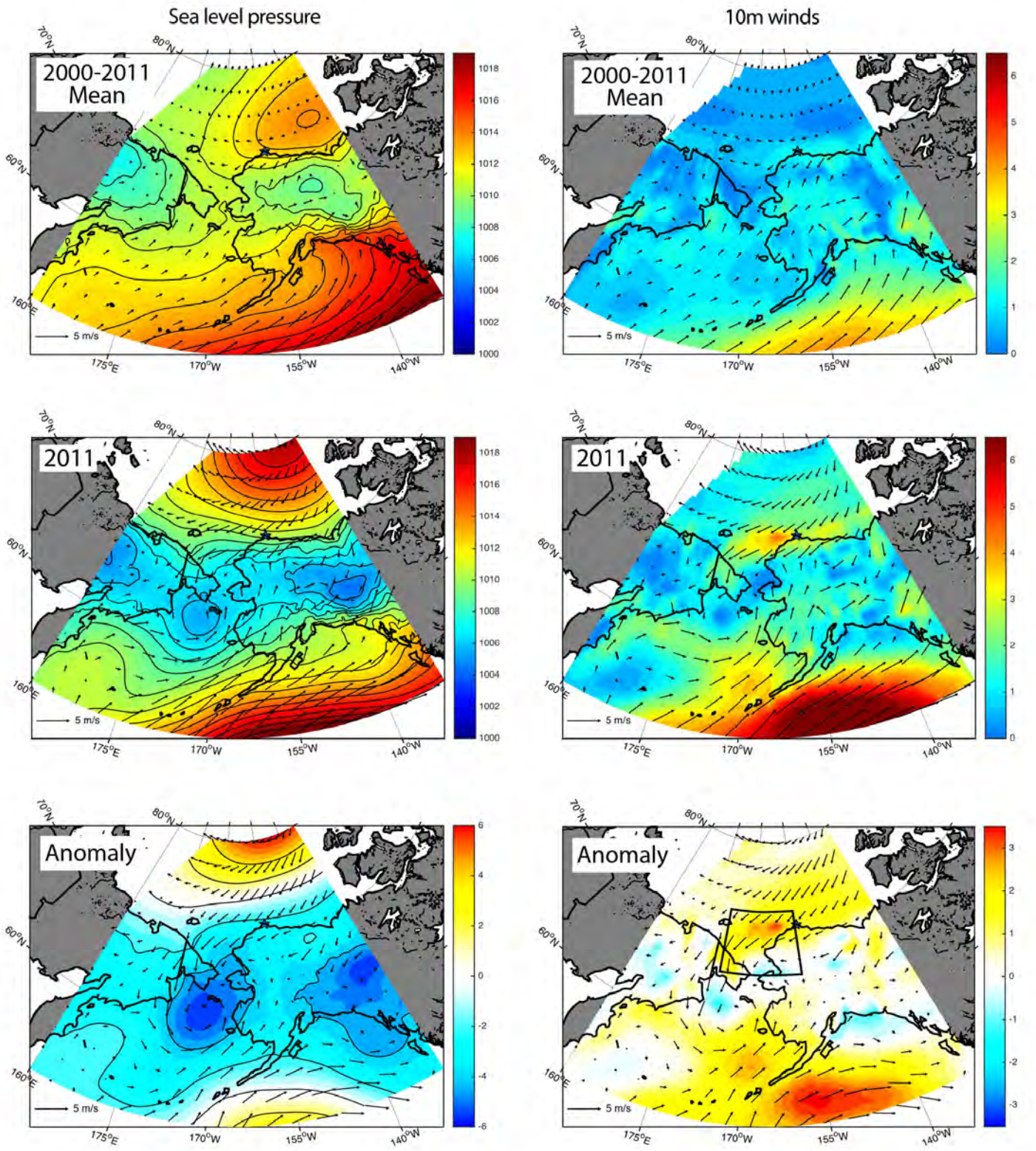

Figure 4: NARR fields averaged over the time period of the ICESCAPE II cruise, 25 June –29 July. The left-hand panels are sea level pressure (color and contours, mb) and 10 m wind vectors. The right-hand panels are 10 m wind speed (color) and 10 m wind vectors. Top row: mean conditions for 2000-11. Middle row: Conditions during 2011. Bottom row: Anomaly (2011 – climatology). The black box in the lower right-hand panel marks the region over which the mean winds were computed (see the text and Figure 5).

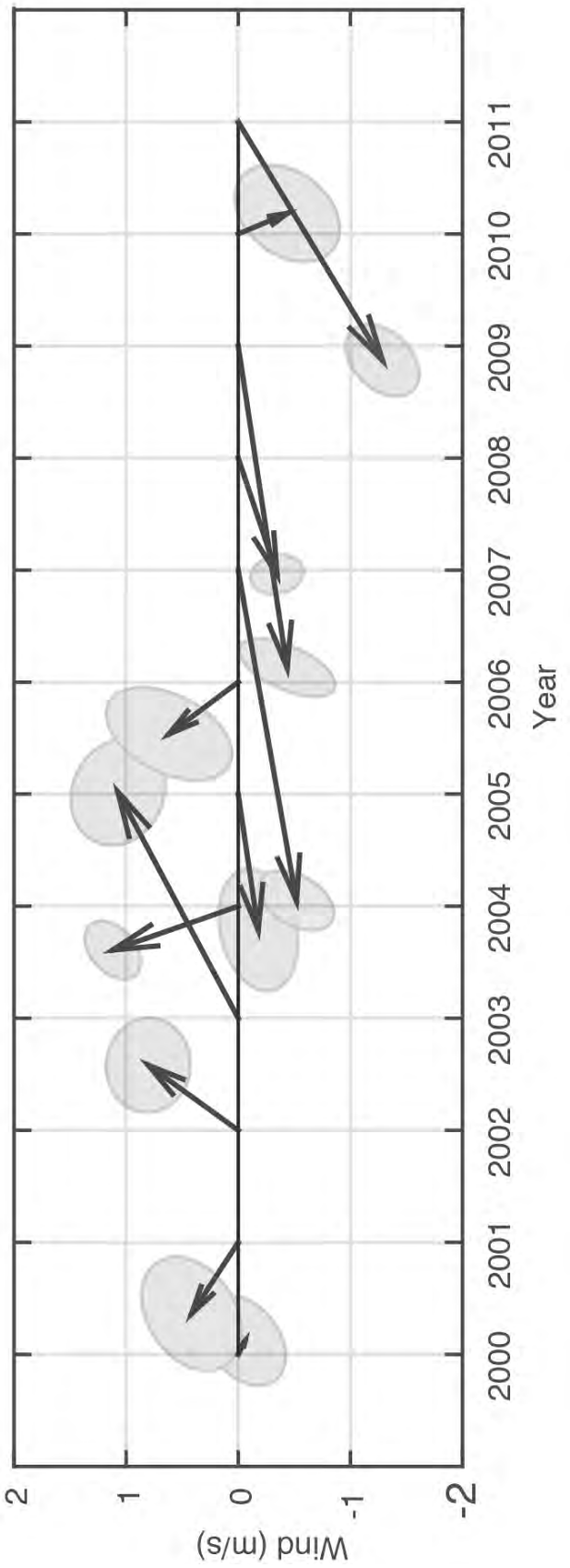

Figure 5: Mean 10 m wind vectors for the Chukchi Sea (within the box shown in Figure 4) over the time period of the ICESCAPE II cruise, 25 June –29 July, shown for each year from 2000-11.

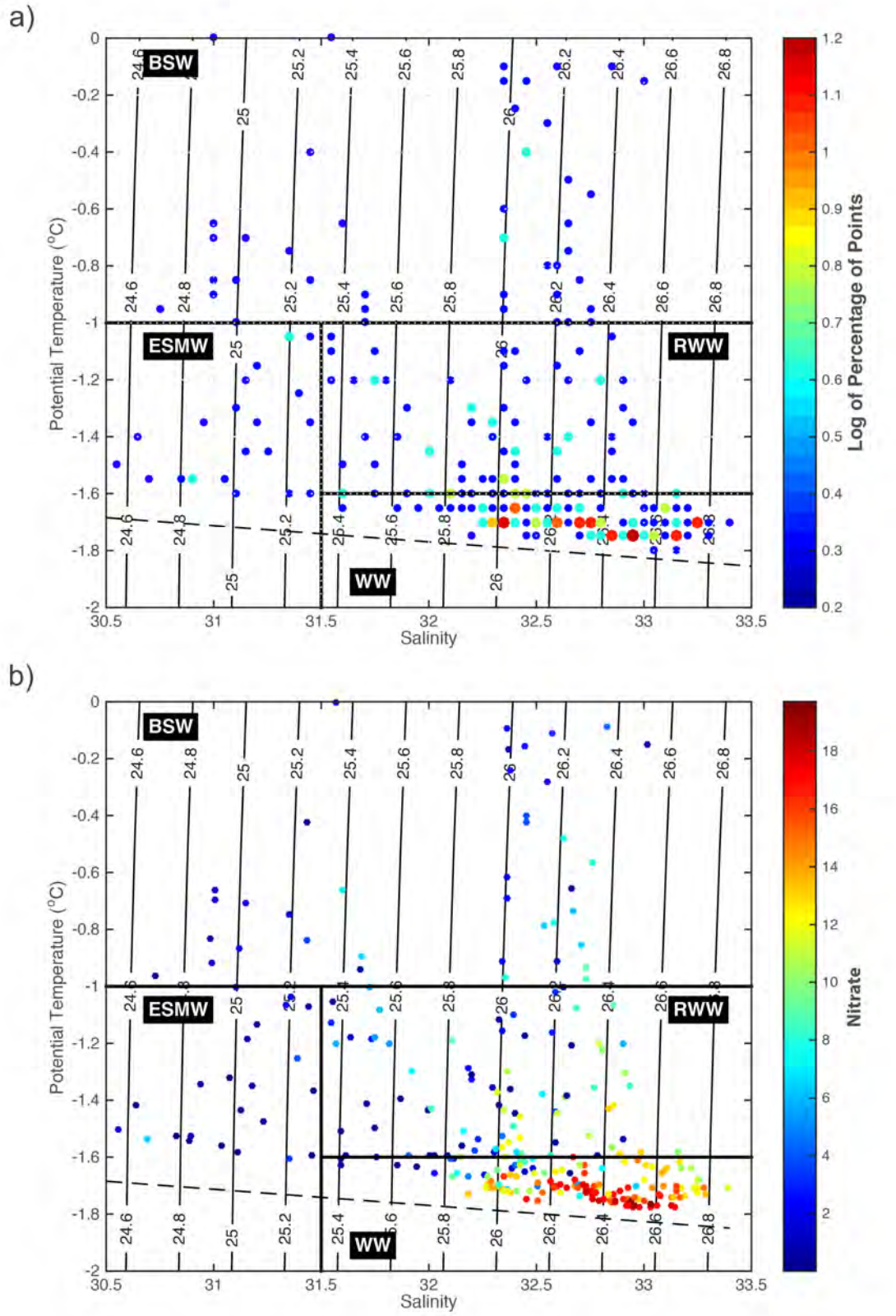

Figure 6: (a) Volumetric T/S diagram using the CTD data from the ICESCAPE II cruise. For each bin corresponding to 0.05°C in temperature and 0.05 in salinity, the number of observations (in log counts) is colored. The thick black lines mark the boundary between the water masses. WW = newly ventilated winter water; RWW = remnant winter water; BSW = Bering Sea Water; ESMW = early season melt water. The thin dashed line is the freezing line. (b) Scatter plot of the bottle data in T/S space where the nitrate concentration is colored (µmol/kg).

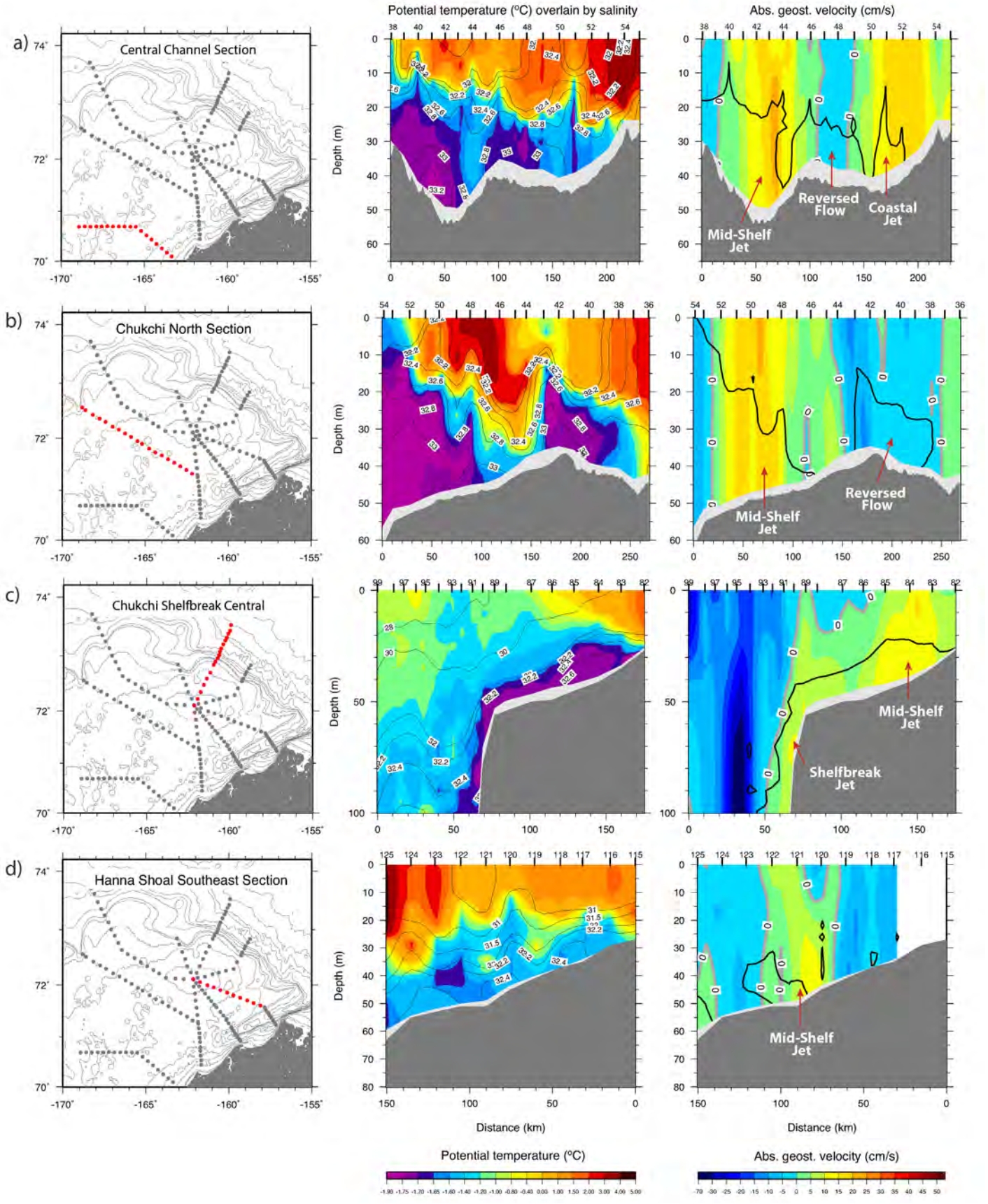

Figure 7: Vertical property sections for selected transects (indicated by red in the left-hand panels). The middle panels show potential temperature (color) overlain by salinity. The right-hand panels show absolute geostrophic velocity (color, where positive velocities are out of the page) overlain by the -1.6°C isotherm (thick black line).

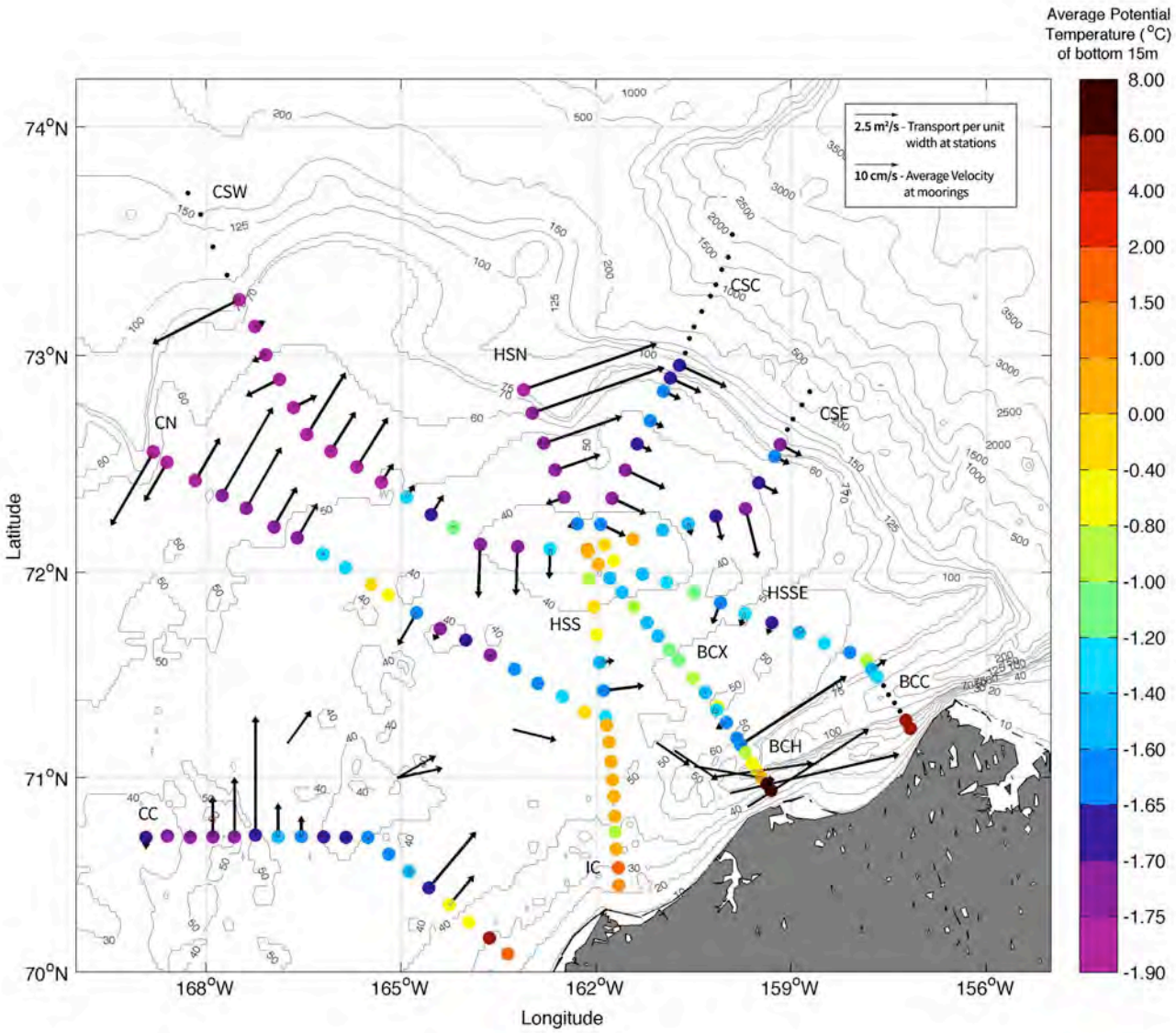

Figure 8: Average potential temperature (color) in the bottom 15 m of the water column at each station whose bottom depth is shallower than 85m. The vectors at the station sites are the transport per unit width of the winter water. The vectors at the mooring sites are the near-bottom velocities (see the legend).

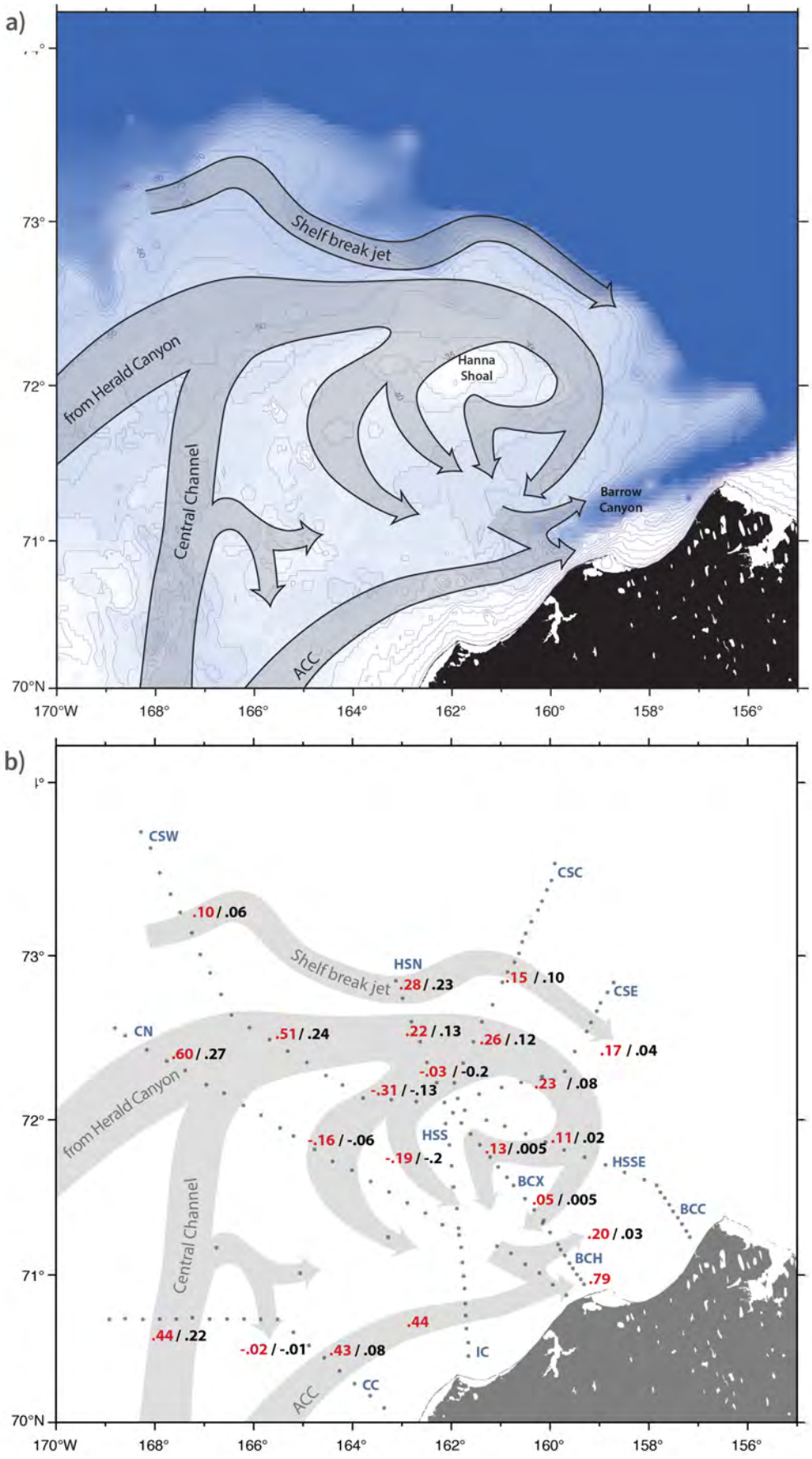

Figure 9: (a) Winter water flow pathways deduced from the data. (b) Volume transports of the pathways. The red numbers are the total transport and the black numbers are the winter water transport. The station locations are marked by the dots.

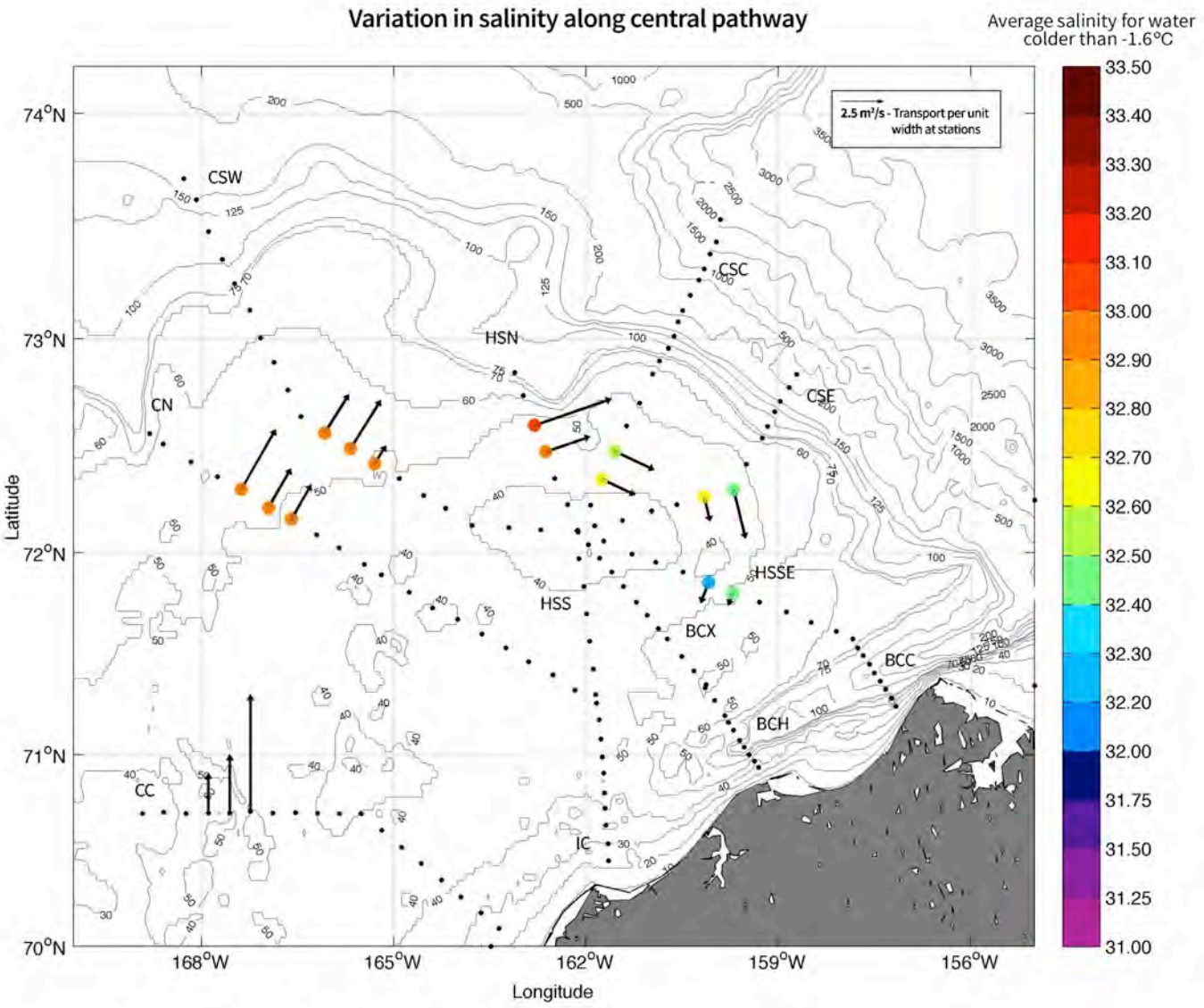

Figure 10: Average salinity (color) of the winter water for the stations comprising the central pathway around the north side of Hanna Shoal. The vectors denote transport per unit width of the winter water (from Figure 8).

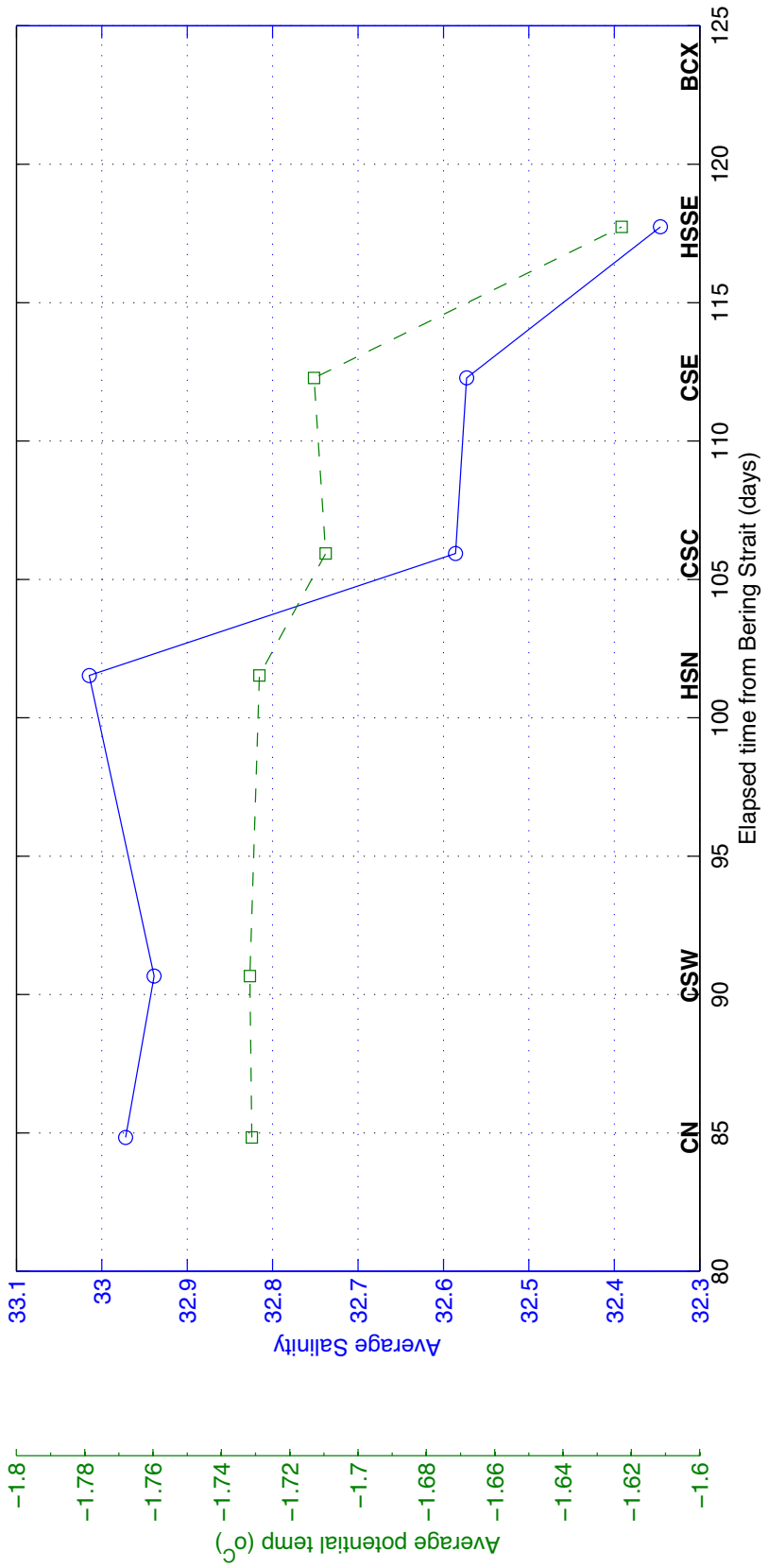

Figure 11: Average salinity and potential temperature of the winter water along the central pathway of Figure 10, plotted versus elapsed time from Bering Strait (see text for details).

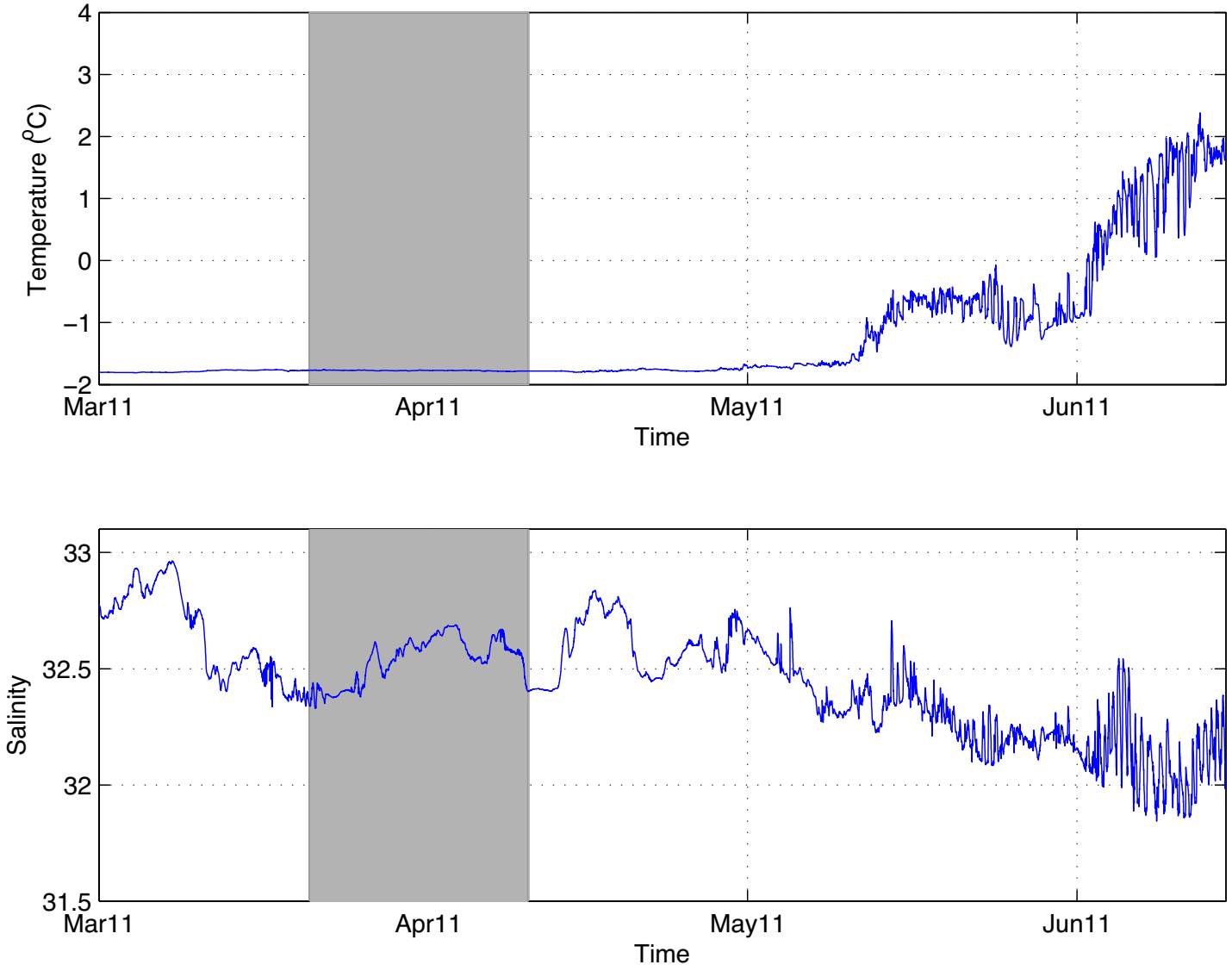

Figure 12: Timeseries of temperature (top panel) and salinity (bottom panel) for mooring A3 in Bering Strait (see Figure 1 for the location of the mooring). The grey shading denotes the time period when the winter water, sampled at the sections in Figure 11along the central pathway, passed through the strait.

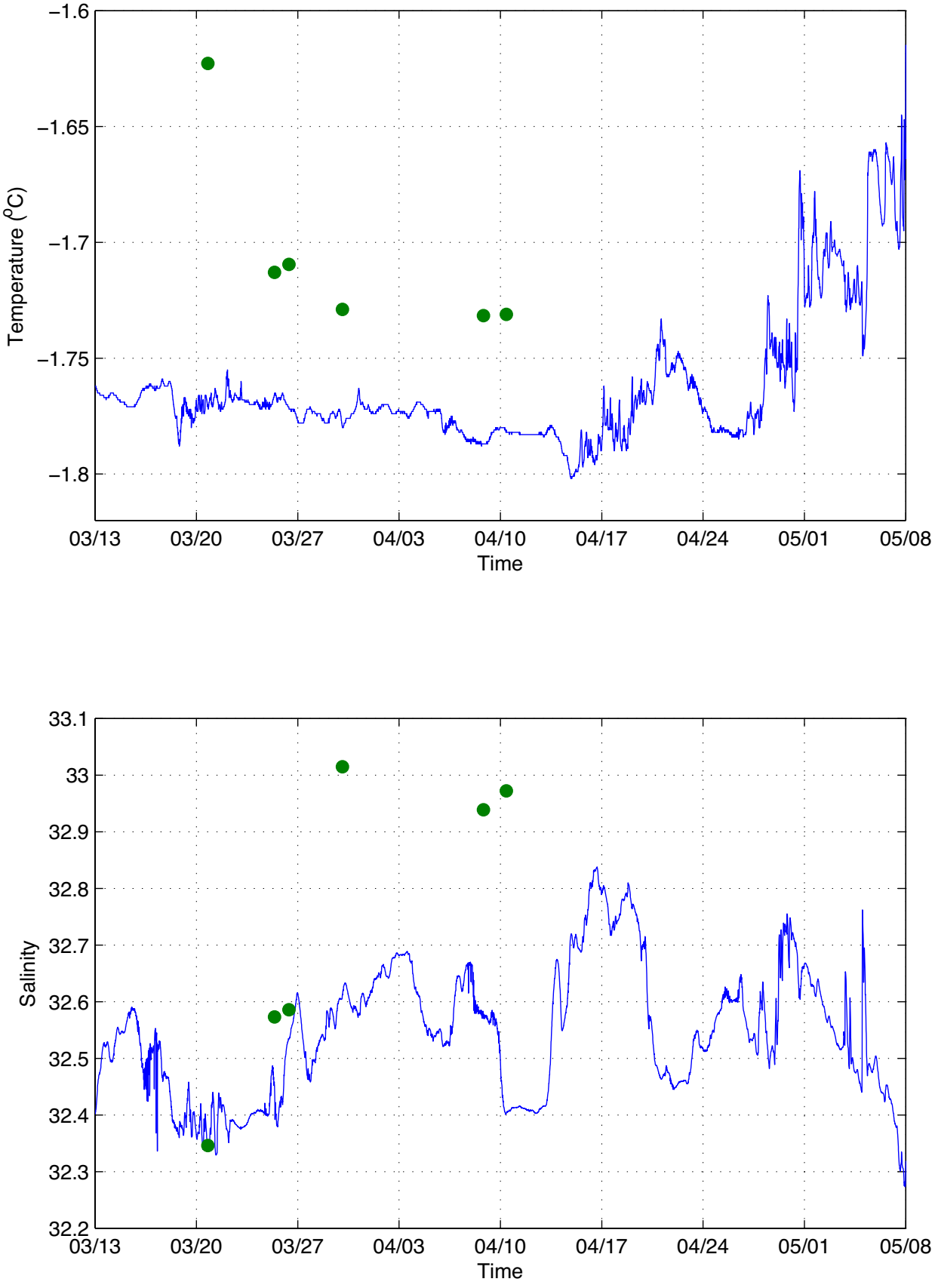

Figure 13: Zoomed-in view of the timeseries of temperature (top panel) and salinity (bottom panel) from Figure 12. The green circles denote the properties of the winter water measured along the central pathway at the sections in Figure 11, adjusted for when the water passed through Bering Strait (see text for details).

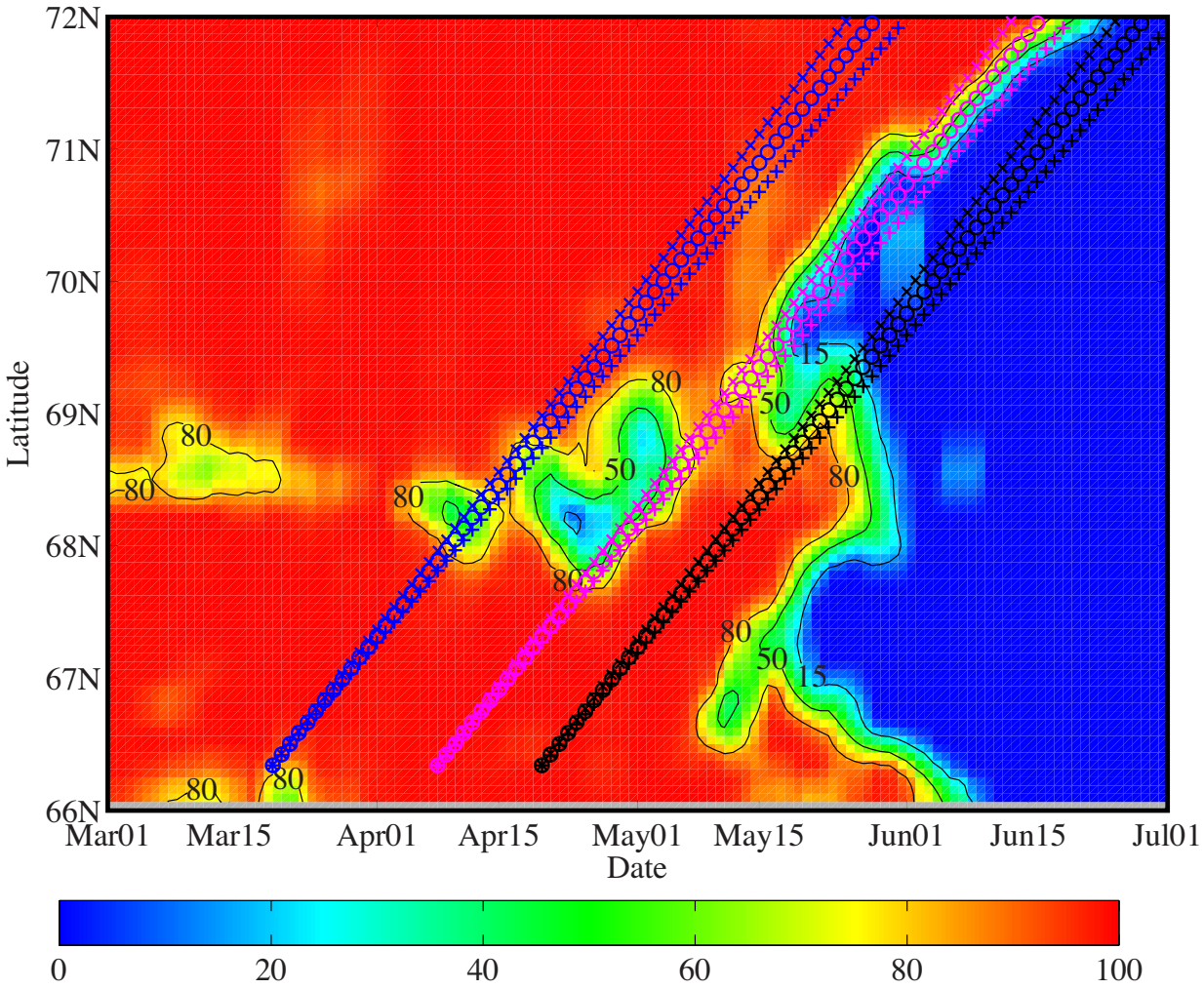

Figure 14: Time-latitude variation of sea ice concentration (%) from the AMSR-E along 167°W during March -July 2011. Also shown are the daily location of parcels starting at 66.3°N on March 20 (blue symbols), April 8 (maroon symbols) and April 20 (black symbols). Locations are shown for parcel velocities of 10 cm/s ('+'), 10.5 cm/s ('o') and 11 cm/s ('x').

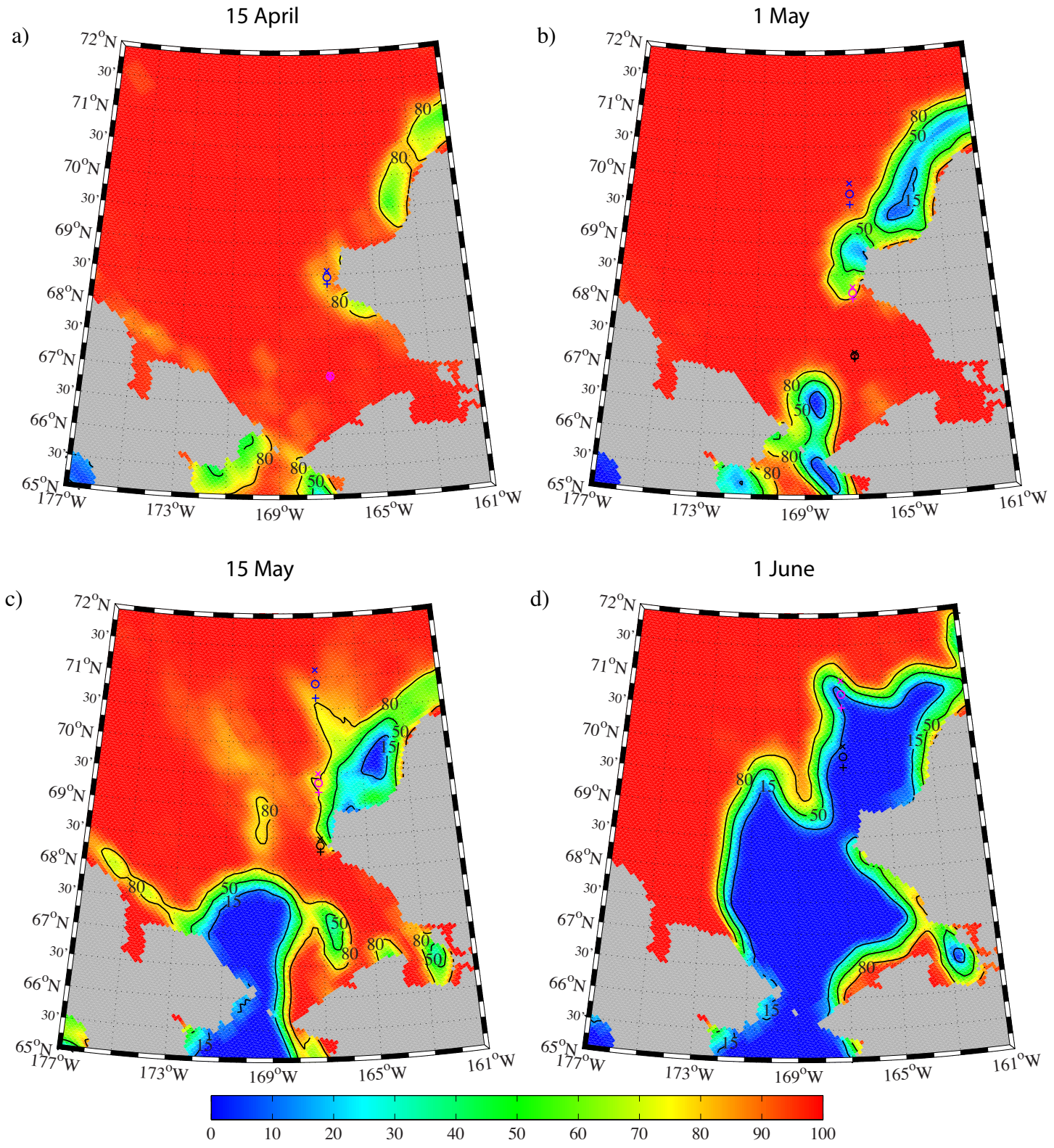

Figure 15: AMSR-E sea ice concentration (%) on: (a) April 15, (b) May 1, (c) May 15 and (d) June 1 2011. Also shown are the locations of parcels starting at 66.3°N on March 20 (blue symbols), April 8 (maroon symbols), and April 20 (black symbols) and travelling along 167°W. Locations are shown for parcel velocities of 10 cm/s ('+'), 10.5 cm/s ('o') and 11 cm/s ('x').

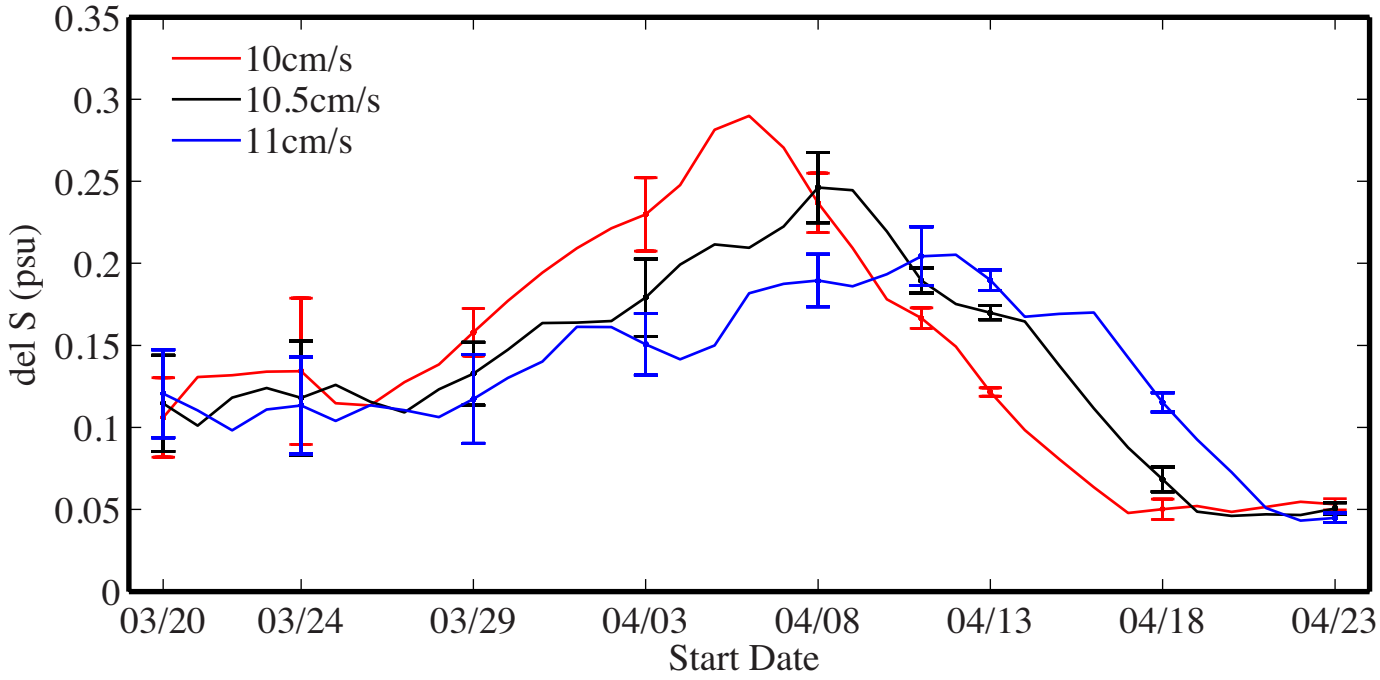

Figure 16: Change in salinity along 167°W for parcels starting at 66.3°N and ending at 72°N as a function of start date in March/April 2011. Changes in salinity are shown for parcel velocities of 10 cm/s, 10.5 cm/s and 11 cm/s. Error bars indicate the change in salinity resulting from a +/-10% change in ice cover along the trajectory of the parcels.

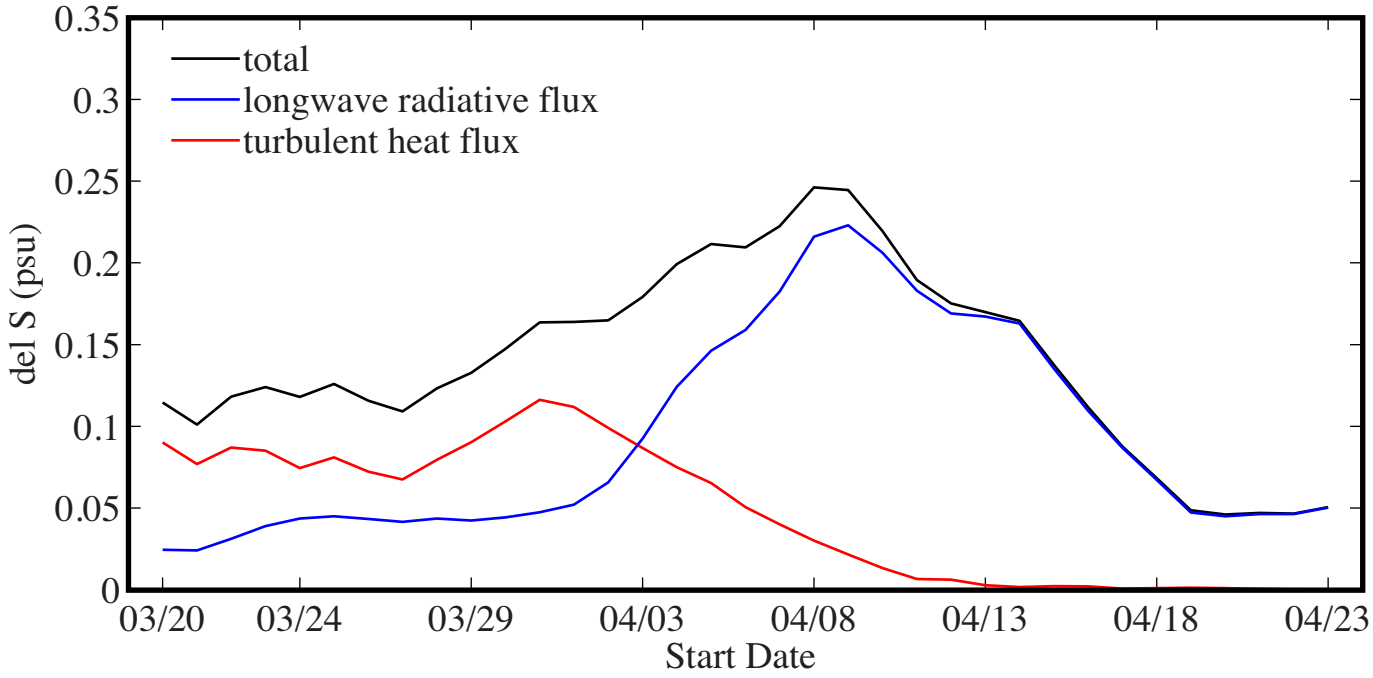

Figure 17: Contribution of the longwave radiative flux (blue curve) and turbulent heat flux (red curve) to the total change in salinity (black curve) along 167°W for parcels with a velocity of 10.5 cm/s starting at 66.3°N and ending at 72°N as a function of start date in March/April 2011.